A STABILITY ANALYSIS OF THE RETAINING WALLS OF MACHU PICCHU

by

Melissa M. Fontanese, E.I.T.

BS in Civil Engineering, University of Pittsburgh, 2007

Submitted to the Graduate Faculty of

the Swanson School of Engineering in partial fulfillment

of the requirements for the degree of

Master of Science

University of Pittsburgh

2010

UNIVERSITY OF PITTSBURGH

SWANSON SCHOOL OF ENGINEERING

This thesis was presented

by

Melissa M. Fontanese, E.I.T.

It was defended on

March 30, 2010

and approved by

Anthony T. Iannacchione, Associate Professor, Civil and Environmental Engineering

Luis E. Vallejo, Professor, Civil and Environmental Engineering

Julie M. Vandenbossche, P.E., Associate Professor, Civil and Environmental Engineering

Thesis Advisor: Luis E. Vallejo, Professor, Civil and Environmental Engineering

A STABILITY ANALYSIS OF THE RETAINING WALLS OF MACHU PICCHU

Melissa M. Fontanese, E.I.T., M.S.

University of Pittsburgh, 2010

The retaining walls of Machu Picchu, constructed of dry stacked granite blocks during the 15th century, have remained standing for centuries in a challenging geologic and climatic setting with little to no maintenance. In order to construct such enduring infrastructure, Incan engineers understood the basic concepts that we use today to design modern retaining walls. A stability analysis, based on conservatively selected parameters, reveals that the Incan walls generally meet modern standards for sliding stability (assuming full-contact and thus maximum frictional forces between blocks) and the walls nearly meet modern standards for overturning stability.

A fractal analysis of the walls, conducted by digitizing and analyzing photos of four retaining walls and one dwelling wall, shows that the roughness of the stones making up the walls is fractal. The analysis also shows that the size distributions of the stones in the walls are fractal over several ranges, or multi-fractal.

The walls were simulated in the laboratory using a matrix of wooden dowels subjected to normal loading via a direct shear apparatus. Force chains formed in the matrix; as the size distribution of the dowels changed with the addition of multiple dowel sizes, the number of dowels not engaged by force chains decreased until all of the dowels were engaged in transmitting the load to neighboring dowels.

The fractal distribution of stone sizes in the walls aids in the transmission of load between individual particles in the wall as demonstrated through the laboratory analysis of

wooden dowels. By engaging each particle in sharing the loading, the full stability of the wall can be realized.

TABLE OF CONTENTS

LIST OF TABLES

LIST OF FIGURES

PREFACE

I would like to thank Dr. Vallejo for mentoring me throughout both my undergraduate and graduate years and for introducing me to the impressive civil engineering achievements of the Pre-Columbian world during my career at the University of Pittsburgh.

I would also like to thank my family, including my parents Blaine and Kimberly Fontanese and my brother Richard, for your patience and encouragement. Thank youyou're your love and support and for encouraging me to pursue a career as an engineer - I couldn't have done it without you.

Thank you to the many mentors I've had so far throughout my career, including Steve Geidel, Alicia Kavulic, Doug Beitko, and Joe Boward. Without their influence, I probably wouldn't even have given geotechnical engineering a second thought.

During my seven years at Pitt, I formed friendships with many amazing young engineers. Thanks to all of you for everything you've done to help me through my academic and professional careers, and above all for being great friends. Thanks to Kara Gamble and Kyra Ceceris for listening to my rants and pretending to understand fractals and retaining walls. We need to plan a trip to Machu Picchu!

Thank you to Dr. Vandenbossche and Dr. Iannacchione for taking the time to review my thesis and sit on the committee, as well as for your support during my years at Pitt.

1.0 INTRODUCTION

1.1 BACKGROUND

The Inca Empire flourished during the 15th and 16th centuries in the Andes Mountains of western South America. The Inca lacked a written language and the technology for the wheel (Wright and Zegarra 2000), but they built extensive infrastructure throughout their territory in the Andes. Roads and bridges to carry foot traffic, retaining walls to support agricultural terraces and buildings, and engineered waterways for irrigation and wastewater were all critical, engineered components of Machu Picchu (ABC-CLIO 2001), which is perhaps the best-known ancient Incan city.

Machu Picchu is located on the eastern side of the Andes Mountains in what is now Peru, east-southeast of Lima near the city of Cusco. Built for the Inca king Pachacuti, it was constructed starting in the middle of the 15th century (ABC-CLIO 2001) on a mountaintop above the Urubamba River. It was abandoned about a century after construction began, around the time the Spanish conquistadors began to occupy South America. The ancient city lay forgotten until Hiram Bingham rediscovered it in 1911 and subsequently published his photos of Machu Picchu in National Geographic magazine (ABC-CLIO 2001).

Figure 1. Map of Peru showing the location of Machu Picchu

Pre-Columbian civilizations are sometimes thought to be primitive, inferior societies in comparison to modern-day civilization. Some of the great achievements of pre-Columbian societies have been credited to extra-terrestrial beings because they appear to be too advanced for such "primitive" cultures to construct. In his book, Chariots of the Gods, Erich Von Daniken (1968) hypothesizes that our planet was visited by extra-terrestrial beings during ancient times. Von Daniken surmises that these visitors were welcomed as gods (as the Spanish Conquistadors were welcomed to the Americas) and many mysterious ancient sites around the world were inspired by or perhaps even constructed by these alien visitors who come from a culture far more advanced than that of our ancestors.

These ancient structures have outlasted many of our modern structures without the benefit of our rigorous mathematical design methods and modern building codes, while demonstrating seemingly modern engineering concepts, such as modular wall construction and

efficient drainage techniques. To this day, major soil movements are problematic in the Machu Picchu region (V. Vilimek, 2006), sometimes so severe that the access route to Machu Picchu is blocked. The Incas managed to build their city in such a way that, even while affected by a multitude of geologic hazards, it remains standing centuries later.

Machu Picchu exemplifies the engineering expertise of pre-Columbian societies. In order to facilitate agricultural activities and create a city high atop a steep mountain in the Andes, the Inca had the ingenuity to construct terraces supported by stone retaining walls. The walls of Machu Picchu have endured centuries of weathering, earthquakes, and various other naturally degenerative processes on a steep mountainside with little to no maintenance. Over five hundred years after construction, the walls are still standing.

Figure 2. Aerial view of Machu Picchu. Note the many retaining walls apparent along the western slope of the site.

Understanding the keys to the longevity of the Incan retaining walls will recognize the intelligence of pre-Columbian societies and contribute knowledge that may improve design and construction techniques for modern retaining walls.

1.2 OBJECTIVE

The objective of this thesis is to investigate the factors that have helped the retaining walls at Machu Picchu to endure for so many centuries and explain some of the mechanisms that may influence their long-term stability, such as: fractal characteristics; formation of force chains; drainage characteristics; and durability of building materials.

This research focuses on comparison of the Incan walls to modern walls and construction techniques, a generalized stability analysis of the Incan walls in accordance with modern standards, fractal analysis using digitized photographs, and laboratory analogy using wooden dowels in a direct shear apparatus to simulate the walls.

2.0 RETAINING WALLS

A retaining wall is a structure that holds back soil in order to facilitate a dramatic vertical (or near-vertical) change in grade. Today, we often use retaining walls to mitigate existing landslides, prevent future landslides, mitigate excessive erosion, support bridge approaches, protect structures, and provide a greater "flat" surface for development. Modern retaining walls fall into several broad categories, discussed in detail in Section 2.1.4, and are engineered to standards specified by building codes to ensure their stability.

The Incas made extensive use of retaining walls at Machu Picchu. The Incan retaining walls were constructed primarily to provide a relatively flat surface for construction of buildings, roads, fountains, other infrastructure, and for agriculture. The Incas lacked a written language and hence, their engineering works were not governed by written building codes as our modern infrastructure is; however, even without the sophisticated knowledge we employ today, they were able to construct an entire city that withstood centuries of neglect and is still standing to this day.

2.1 STATE OF THE ART

2.1.1 Retaining Wall Design Methodologies

From a geotechnical standpoint, retaining walls are typically designed to an appropriate factor of safety for bearing, sliding, and overturning. A factor of safety is defined as the ratio of the sum of forces resisting failure to the sum of forces causing failure. The forces which typically cause retaining wall failures include the lateral pressure imposed by the soil supported by the wall, the weight of surcharge loads such as roadways or structures, and hydrostatic pressure (described further in Section 2.1.2). Forces resisting failure of the retaining wall may include the weight of the wall, the friction developed along the wall-soil interface, the passive resistance generated by the soil in front of the wall, and the resistance generated by anchors or other appurtenances, depending upon the type of retaining wall in question.

A factor of safety below 1.0 (the sum of the forces causing failure is greater than the sum of the forces resisting failure) indicates failure of the structure and a factor of safety equal to 1.0 (the sum of the forces causing and resisting failure are equal) indicates a marginally stable structure which is at equilibrium. At equilibrium, any small disturbance to this structure which adds to the sum of forces causing failure will lead to failure of the structure.

Due in part to the marginal stability of a structure at a factor of safety of unity, retaining walls and other structures are typically designed to a factor of safety greater than one, specified by a building code or other local standard of care, in order to ensure the stability of the wall. By including a factor of safety in the design process, the inherent variability in strength of construction materials and the earth supporting and being retained by the wall is offset.

Structurally, the materials used to construct the retaining wall are typically checked for strength and elastic deformation, at a minimum.

Several design methodologies have been employed in the design of retaining walls and are selected based upon the local standard of care and type of retaining wall being designed. The "state of the art" typically governs for the particular material type; traditionally steel retaining walls were designed using allowable stress design (ASD) and concrete walls were designed using ultimate strength or load factor design (LFD). Load and resistance factor design (LRFD) is becoming increasingly popular for design (it is currently the state of the art for steel structures).

ASD compares the actual loads imposed on structural components to predetermined allowable loads. These allowable loads are based on widely-accepted material strengths gleaned from laboratory tests, to which a reduction factor is then applied thus providing a factor of safety. Allowable loads/material strengths and appropriate factors of safety are governed by various codes specific to the wall purpose and geographic/political regions.

While ASD applies a reduction factor to the strength of the material in question, LFD applies a factor to the load on the structure. This factor increases the apparent magnitude of the load, building the factor of safety into the load used for the design. As with other design methodologies, the appropriate load factors and factors of safety are dictated by codes and the local standard of care.

LRFD has become an increasingly popular design method in recent years and is preferred in the realm of highway design. LRFD, a hybrid of the ASD and LFD methodologies, examines a variety of limit states (reflecting the various conditions under which the structure must remain stable). Load factors (greater than 1.0) are assigned to the loads imposed on the structure, similar to LFD, and resistance factors (less than 1.0) are applied to the material properties of the

structure components, similar to ASD. Load and resistance factors are determined via statistical analyses and are dictated by the applicable regulatory code.

2.1.2 Drainage and Hydrostatic Pressure

Functional drainage systems are critical to the long-term stability of retaining walls. When water collects behind a retaining wall, it builds up excessive hydrostatic pressure behind the wall and adds very large additional, often unanticipated (and thus unaccounted for during the design process) loads to the wall. Hydrostatic pressure buildup can lead to catastrophic failures of retaining walls.

To mitigate the buildup of hydrostatic pressure behind retaining walls, drains (backfilled with a free-draining material) are usually located immediately behind the retaining wall and the drained water is discharged via a weep hole in the face of the wall. Special care must be taken to make sure that this water is diverted to an appropriate location; water ponding in front of a retaining wall adjacent to a roadway can cause hydroplaning and ice hazards to motorists or may lead to excessive softening of the subgrade and ultimately unanticipated settlement of nearby structures.

2.1.3 Changes in Wall Type Preferences

As socioeconomic and materials science factors have changed, so has the preferred type of retaining wall. Cost is one of the most important factors considered when determining the appropriate type of wall for a specific project.

Historically, the cost of materials drove the cost of a civil engineering project. Labor was plentiful and relatively inexpensive; construction materials required massive amounts of energy to produce and were relatively expensive to manufacture. Many historic civil engineering projects were focused on minimizing the amount of material required for construction and were less focused on minimizing the labor required to build it. Cast-in-place walls, requiring very little prefabrication and more on-site labor, were common due to the economic circumstances of the time.

As labor movements advanced, the cost of labor rose; conversely, more efficient automated manufacturing processes have decreased the cost of prefabricated construction materials. Modular precast concrete walls have recently become increasingly popular as they can both be inexpensively manufactured and require minimal labor to construct.

2.1.4 Types of Retaining Walls

Modern retaining walls can generally be classified as gravity/semigravity walls, cantilever walls, non-gravity cantilever walls, anchored walls, and mechanically stabilized earth walls. Retaining walls can be considered solely one of the aforementioned wall types or a hybrid of multiple wall types.

A specific wall type is chosen for a particular project based on:

- the characteristics of the site soils and bedrock. Some walls are better suited to a relatively shallow bedrock surface while others will perform just as well in a thick soil mantle. Soft soils may induce bearing capacity and settlement concerns. Very hard rock layers may make rock excavation (for particular types of walls) impractical. Chemical characteristics of the soil may dictate that

specific materials be used to construct the retaining wall to mitigate corrosion concerns.

- physical and spatial site constraints. The size and orientation of a site may dictate the type of wall that will be constructed; some walls require relatively large construction areas while others can be built in a relatively small area. The location of overhead or buried utilities may dictate what type of wall may be constructed – relocating utilities can be dangerous, inconvenient, and expensive; it may be more cost-effective to choose a wall that can work around utilities rather than relocating them.
- economic factors. Financial concerns often impose the majority of restrictions on a project; not only does the owner wish to preserve the budget, he or she would like the best product they can have for the lowest price possible.
- aesthetic considerations. The look of a wall is especially important when located in an area where it will frequently be seen, for example: a wall supporting a hillside behind a building; above a road; near a home; or in a scenic area. In recent years, concrete has been used for many aesthetic touches – walls can be made of colored and/or stamped concrete, mimicking a stone wall or rock cut.

2.1.4.1 Gravity and Semigravity Retaining Walls

Gravity walls are massive walls that utilize only their own weight in holding back soil. The walls at Machu Picchu fall under the umbrella description of gravity walls. Gravity walls are commonly constructed of dry stacked or mortared stones, precast concrete blocks, cast-in-place concrete masses, or wire mesh gabions filled with stones, among other materials. Semigravity retaining walls are made of reinforced concrete (steel reinforcing increases the

structural strength of the wall, reducing the required section). For the purpose of discussion herein, semigravity walls will be considered a type of gravity wall.

Figure 3. A gravity wall made of stacked precast concrete blocks with keyways.

As previously discussed, proprietary “modular” walls have become popular in recent years and are used for everything from backyard landscaping to roadway construction. Blocks for modular walls come in a variety of sizes and finishes to suit both the engineering and aesthetic requirements of the wall. They are sometimes held together with interlocking keyways or dowels to provide some resistance to toppling failure. Machu Picchu’s retaining walls can be considered modular walls in the sense that they are a large mass constructed of numerous

individual units, although they are not uniform, manufactured units like those of modern modular walls.

Gravity walls are generally inexpensive relative to more complex retaining walls because they can frequently be constructed without the use of sophisticated equipment and from fairly common and easily procured construction materials; however, certain types of gravity retaining walls, such as those made of wire mesh gabions filled with stones, can be fairly labor-intensive to construct. As mentioned before, today's construction projects tend to favor fast-paced construction and minimal labor. As such, today's projects favor modular, prefabricated units that are uniform and easily assembled.

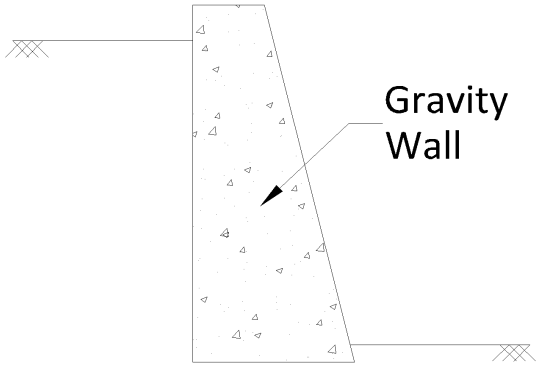

Figure 4. Schematic drawing of a gravity retaining wall

From a practical standpoint, the height of a gravity wall is limited. The only force resisting failure is the weight of the wall itself, which has to resist the force of the soil it retains. The taller the wall, the larger the mass of soil being retained; the more mass being retained by the wall, the heavier the wall must be to resist sliding and overturning. For a very tall gravity wall, it is difficult to achieve an acceptable factor of safety against sliding and overturning; in order to create a wall massive enough to retain such a large volume of soil, the wall must be made so thick that it would be impractical to construct. The wall may not fit within the

boundaries of the site or the volume of material required to produce a stable retaining wall may be cost prohibitive. The weight of such a large retaining wall can lead to bearing capacity failures and/or excessive settlements in the soil underlying the wall.

Most retaining walls built by homeowners are gravity walls. Homeowners generally employ them to retain a yard superjacent to a depressed driveway, for decorative purposes in a garden, or for other landscaping projects. They are relatively inexpensive for projects of such a small magnitude and there are many contractors who are familiar with the appropriate construction techniques; a homeowner may be able to construct a small modular wall on his own, which can be a substantial cost savings over hiring a contractor to build it. Gravity walls can easily be aesthetically pleasing – they may be made of stamped concrete which can be formed to nearly any pattern the owner desires.

Figure 5. An example of a decorative concrete finish on a wall. (Photo property of Boulderscape, Inc., and Soil Nail Launcher, Inc.)

2.1.4.2 Cantilever Retaining Walls

Cantilever walls resemble gravity walls, but with a cantilever arm added to the wall in order to employ the weight of the retained soil in maintaining the stability of the retaining wall in addition to the weight of the wall itself. Cantilevered walls are often shaped like an upside-down "T" or "L". Because of the added resistance from the cantilever, these walls usually require less material than traditional gravity walls. They are typically made of cast-in-place, steel-reinforced concrete.

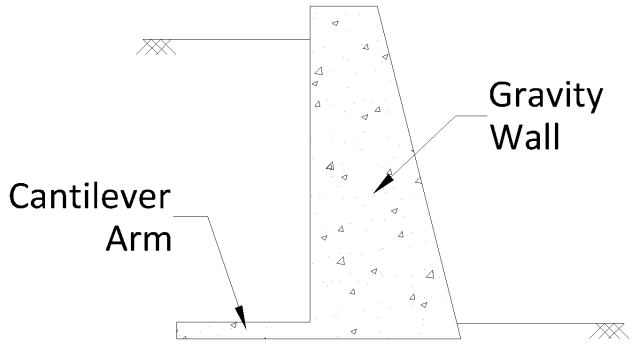

Figure 6. Schematic drawing of an L-shaped cantilevered retaining wall

The cantilever arm gives this wall several advantages over a traditional gravity wall. The weight of soil behind the retaining wall pushes down on the cantilever arm, creating a force that resists overturning of the wall. The cantilever arm also increases the surface area of the base of the wall, increasing the wall's sliding resistance. From a functional standpoint, these additional forces allow cantilever walls to function effectively over greater heights than traditional gravity retaining walls. Cantilevered walls sometimes include counterforts (struts connecting the actual wall to its cantilever arm) to reduce the required wall section. Thus, cantilever walls can typically be made taller and more slender than their pure gravity wall counterparts.

In order to facilitate construction of the cantilever arm, a larger excavation is required relative to that required for a traditional gravity wall. Depending upon the site geometry, especially in instances where limited right-of-way or the location of a buried utility line is an issue, additional excavation can be a deterrent when evaluating the suitability of a cantilever wall. In order to provide a safe workspace, the excavation sidewall should be sloped back, requiring even more space, or temporary shoring should be installed. Installing temporary shoring is essentially building another wall just to facilitate the construction of the actual wall. This may be deterrent due to its impacts on project finances and schedule.

In addition, the cantilevered wall is subject to the same practicality drawback as a traditional gravity wall: beyond a certain height, the wall will have to be so massive that it may be more cost- and space- effective to choose another wall type for the project.

2.1.4.3 Non-Gravity Cantilevered Walls

Non-gravity cantilevered walls are usually walls with continuous vertical elements (like steel sheet piles) or walls with discrete vertical elements (like soldier beam and lagging walls). Non-gravity cantilevered walls are constructed one of two ways: top-down or bottom-up. "Top-down construction" implies that the wall is constructed from the top, down; in the case of a wall on a slope, the wall can be constructed from the top of the slope, eliminating the need for excavating a construction bench. Excavating a bench for bottom-up construction can be risky, particular on a hillside, as the excavation may disturb the toe of the slope and possibly induce a slope failure. A bench may also require temporary shoring, which will add additional cost to the project. Top-down construction eliminates, or at the very least minimizes, the need for risky and/or costly excavations. After constructing the wall, the soil in front of it can be excavated to

final planned grade; thus the retaining wall fills two roles: the role of temporary shoring for the excavation and its intended role as a finished-product retaining wall.

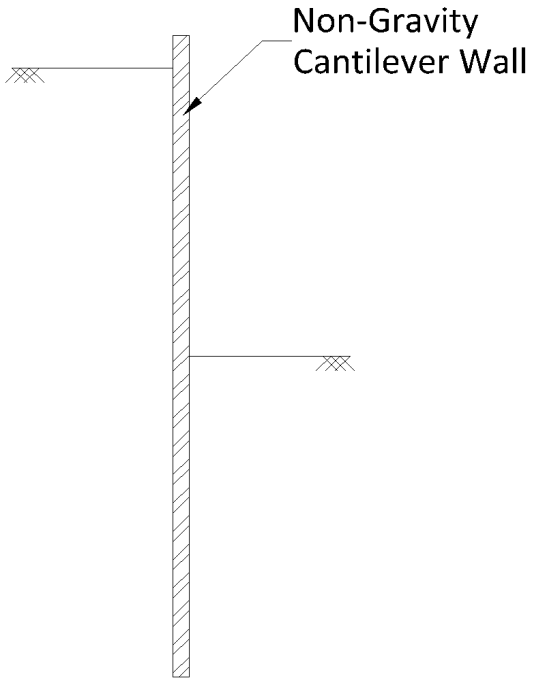

Figure 7. Schematic drawing of a non-gravity cantilever wall

Sheet pile walls are constructed by driving sheet piling made of steel, wood, or vinyl into the ground. Soldier beam and lagging walls are constructed by installing steel H-piles or wide-flange beams spaced at a specified interval (by driving them into the ground or by drilling a shaft and grouting them in place) and then installing concrete or wooden lagging between the piles. The lagging retains the soil and is held in place by the steel piles. As a rule-of-thumb, non-gravity cantilevered walls generally extend to depths of twice the exposed height of the wall (Das, 2004). These walls are especially useful in "cut" situations because they can be installed via the top-down method before the excavation takes place, eliminating the need for temporary shoring during excavation.

Non-gravity cantilever walls are generally fairly expensive relative to gravity and cantilever walls because construction frequently requires the use of expensive heavy machinery, including cranes and large drill rigs. They are especially useful in areas with limited construction space, such as a failing slope subjacent to a roadway, because they can be installed via the top-down method. These walls have relatively small "footprints" and thus it is easier to avoid conflicts with existing buried utilities during construction.

Figure 8. A soldier beam and lagging wall supports a roadway and several buried water mains along a stream in Sewickley, Pennsylvania, constructed via the top-down method.

Aesthetically, both sheet pile walls and soldier beam and lagging walls can have a very sterile, industrial appearance which may not be desirable for certain applications. In applications where appearance is important, walls can be covered with an architectural veneer to give the

desired appearance. In the case of soldier pile and lagging walls, concrete lagging can be colored and/or stamped to give a natural look or an artistic finish.

2.1.4.4 Mechanically Stabilized Retaining Walls

Mechanically stabilized earth walls are essentially specialized gravity walls which employ strips of galvanized metal, geotextile, or similar manufactured mesh between compacted lifts of soil faced with a skin (usually made of concrete). By reinforcing lifts of soil with manufactured reinforcing strips or geofabrics, the soil's shear strength is increased, and these lifts work together as one large mass of soil. These walls are typically constructed with granular rather than fine-grained soils for drainage purposes, thus reducing the risk of soil-weakening excess pore water pressure buildup.

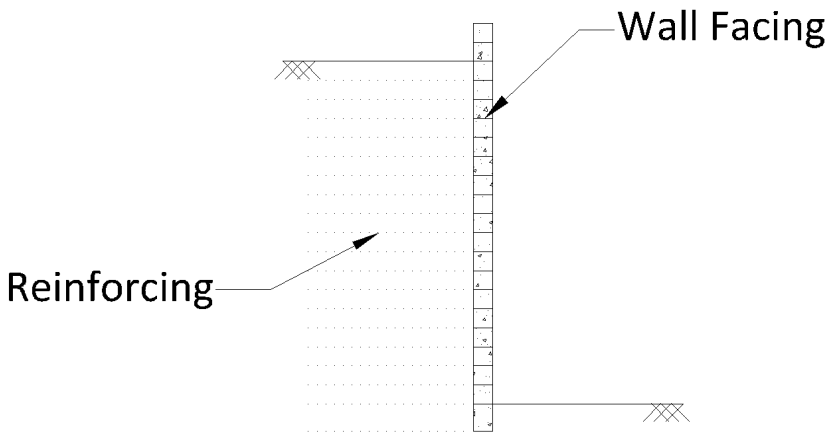

Figure 9. Schematic drawing of a mechanically stabilized earth wall

In addition to the typical design criteria of overturning, sliding, and bearing capacity (all related to the external stability of the wall), mechanically stabilized earth walls must be checked for internal stability. Internal stability for a mechanically stabilized earth wall relates to the strength of the reinforcement (it should be designed to resist both pullout and tensile failures)

and the condition of the wall facing. The type of reinforcing used between layers of soil can have a dramatic effect on the performance of the wall; metal strips, even when properly drained, can be affected by oxygen and moisture in the soil and corrode, potentially leading to premature failure of the structure.

Figure 10. Settlement may induce failures in mechanically stabilized earth walls. (Photo property of J. Boward)

A common mode of failure for mechanically stabilized earth walls is bearing capacity or settlement. If the compacted soil is placed atop a weaker soil subgrade, the surcharge of the wall may cause settlement in the subgrade and ultimately cause damage to the wall. If the lifts of soil making up the wall are not properly compacted, the lifts may settle. Both of these types of

failures can cause distresses to the reinforcement and ultimately cause the wall to catastrophically fail.

Whereas non-gravity cantilevered walls are best suited for “cut” situations, mechanically stabilized earth walls are ideal for “fill” situations, such as highway embankments and bridge approaches. These walls are especially useful in highway construction for fill embankments where limited right-of-way does not permit the use of a slope.

2.1.4.5 Anchored Walls

Any type of retaining wall can be considered an anchored wall if additional support is added to the wall by anchoring it back into the retained soil or into bedrock. Anchors increase the capacity of the wall, thereby reducing the required section and allowing taller walls to be constructed.

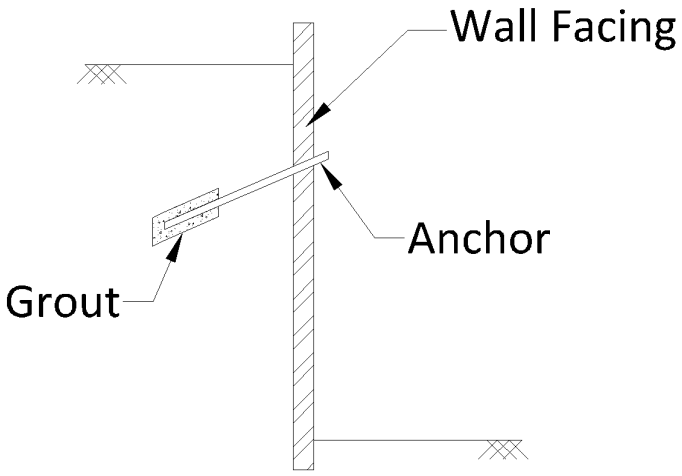

Figure 11. Schematic drawing of an anchor wall with a tieback.

Two general categories of anchors are employed in retaining wall construction: deadman anchors and tiebacks. Deadmen are usually concrete blocks (precast or cast-in-place) attached to

the wall with a tie-rod or strut. Tie-rods/struts are attached to the face of the wall with a wale. The deadman anchor works by gravity combined with the lateral passive pressures generated by the soil in front of the anchor. Deadman anchors and their Rankine passive zones must be located outside of the Rankine active zone behind the wall to realize the full resistance of the anchor. Should the anchor be located completely within the active zone, the anchor will do essentially nothing to assist the retaining wall in holding back the soil because it is located within the wedge that is "moving along" with the wall as it moves.

Figure 12. Tiebacks used to strengthen a failing retaining wall in Pittsburgh, Pennsylvania. (Photo property of J. Boward)

Tiebacks are steel cables or bars which are grouted in place. During construction, a hole is pre-drilled to a specified depth, the steel is inserted into the borehole, and the borehole is then pumped full of grout. The grout forms a grout bulb which serves to bond the steel tieback to the

soil or rock. Tiebacks may be tensioned during installation or tension may develop as load is applied to the tiebacks.

Adding anchors to a non-gravity cantilevered wall can dramatically decrease the required embedment depth and required section, saving on both materials and labor time; however, installing anchors can be quite costly. They can make a geometrically impractical wall option a more practical solution by reducing the required size of the wall. Anchors can sometimes be used to "shore up" a failing retaining wall, as shown in Figure 12.

2.2 THE RETAINING WALLS OF MACHU PICCHU

The retaining walls found at Machu Picchu are gravity walls. The walls are constructed of various sizes of stones, ranging from very massive stones (several feet in diameter) to smaller stones (several inches in diameter). The Incas built solid foundations in the slope's colluvial soil from large stones or by building directly on top of exposed bedrock (Wright and Zegarra). The walls of the agricultural terraces, studied herein, have a batter of approximately 5%. Several layers of soil were used to backfill the walls: a base layer of gravel underlying a layer of fine sand and gravel, capped with a topsoil layer used for growing crops. The stacked stones continue below grade as a foundation system.

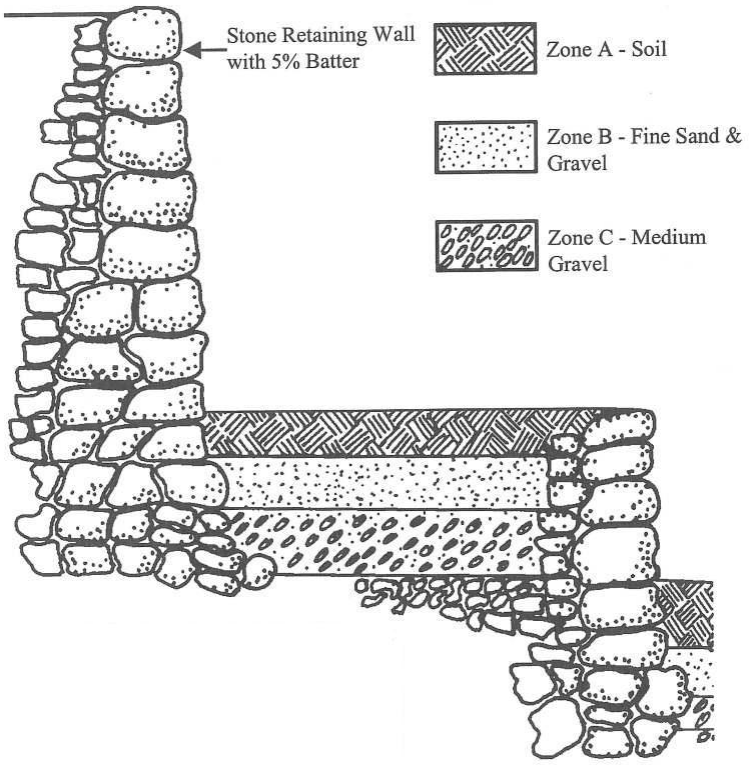

Figure 13. A cross-section of an agricultural terrace at Machu Picchu (Wright and Zegarra, 2000)

The Inca engineers understood the importance of effective drainage. The walls were backfilled with layers of soil that increased in coarseness with depth to prevent the topsoil from washing away (the change in gradation forms a sort of filter). The walls studied herein are dry stacked walls that do not perfectly interlock – this allows excess water to weep out of the front of the wall. Other nearly perfectly-interlocking walls were provided with weep holes, such as the Artisans Wall (Wright and Zegarra). Drains constructed behind the walls were filled with rock chips generated during stone cutting operations for the construction of the city. These drainage measures reduce hydrostatic pressure buildup behind the walls and increase the long-term stability of the city's walls.

The retaining walls were constructed from granite blocks. Granite, a hard igneous rock, is well-known for its durability and is used in a multitude of construction projects ranging from

the walls of Machu Picchu to architectural treatments for buildings to kitchen countertops. Had the walls been constructed from sedimentary rocks, such as sandstone or siltstone, perhaps the bonds cementing the individual particles in the rock together would have succumbed to the moist climate of Machu Picchu long ago.

Of all the retaining walls at Machu Picchu, the agricultural terraces seem to have been constructed with the least concern for aesthetics. Their stones were not carefully carved to interlock like puzzle pieces or shaped into uniform blocks, but were irregularly shaped and of greatly varied sizes. Perhaps the Incan engineers made a conscious decision to build walls in this manner because they thought it would bring greater stability to the walls, or perhaps it was a matter of convenience. Rather than taking the time and effort to perfectly carve each and every stone, they could use "leftovers" from other projects or at the very least, minimize the "fabrication time" - time spent quarrying and shaping stones - for the wall units. This variety of shapes and sizes of individual stones may be one of the keys to the stability of the Incan walls, along with effective drainage, and proper foundations. In Chapter 3.0, the stability of the walls at Machu Picchu will be analyzed quantitatively.

3.0 STABILITY ANALYSIS

As discussed in Chapter 2.0, today's retaining walls are generally designed to meet three criteria: resistance to sliding, resistance to overturning, and adequate bearing capacity. This chapter will further discuss each of these failure modes and use modern engineering analysis to demonstrate the stability of the Incan retaining walls.

3.1 MODERN RETAINING WALLS

3.1.1 Sliding

A sliding failure occurs when the horizontal forces pushing against the retaining wall overcome the horizontal forces holding the retaining wall in place and the wall is displaced forward along the ground surface. In dry stacked walls, individual wall units may slide with respect to one another (a "popout"-type failure) and cause a portion of the wall to fail.

The factor of safety against sliding along the base of a retaining wall is defined by the ratio of the forces resisting sliding to the forces driving sliding and can be expressed as

$$FS_{sliding} = \frac{\Sigma F_R}{\Sigma F_D} \qquad \text{(Equation 3.1)}$$

A factor of safety against sliding equal to 1.5 is commonly used in design.

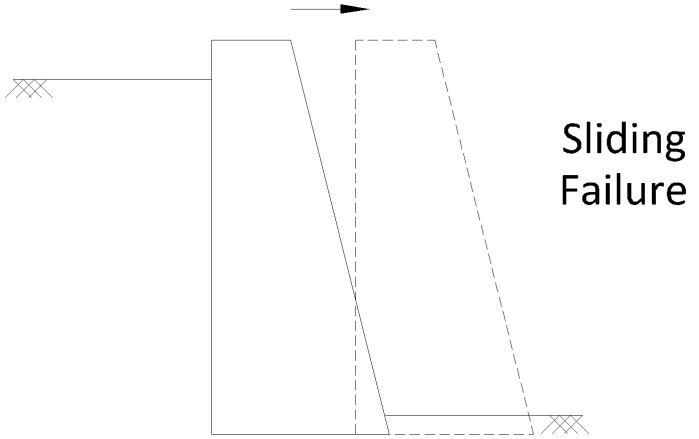

Figure 14. Illustration of sliding failure.

The force causing sliding in the case of the Incan walls (and other gravity walls) is the horizontal pressure exerted by the soil and water pressure behind the wall. The resisting forces include friction between the base of the wall and the soil, and the passive pressure generated by the soil in front of the toe of the wall. Mechanically stabilized earth walls, like gravity walls, achieve their resistance to sliding via the friction generated along the base of the wall. In the case of cantilevered retaining walls, additional frictional resistance is achieved by the greater surface area of the base of the wall (relative to traditional gravity walls. Non-gravity cantilevered walls overcome sliding failure by amassing a large quantity of passive earth pressure in front of the wall. Anchored walls achieve greater sliding resistance via horizontal forces generated by the anchors, in addition to friction along the base of the wall and/or passive pressure generated by the soil in front of the wall.

Figure 15. A "popout" failure in a gravity wall in Edgeworth, Pennsylvania. (Photo property of J. Boward)

3.1.2 Overturning

Overturning failure occurs when the forces pushing against the wall cause it to rotate about its toe, tipping it over. Smaller-scale toppling failures tend to occur in modular dry-stacked walls, whereby the individual units making up the wall may overturn, causing just a portion of the wall to fail.

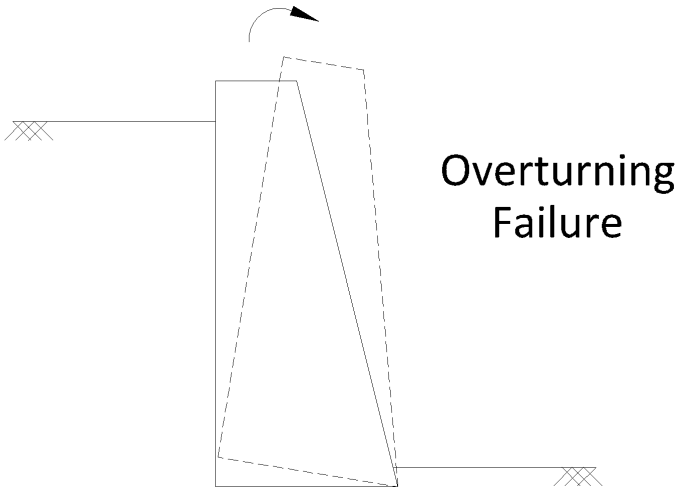

Figure 16. Illustration of overturning failure.

The factor of safety against overturning is calculated by the ratio of the moments about the toe of the wall tending to resist overturning to the moments about the same point driving overturning and can be expressed as

$$FS_{overturning} = \frac{\Sigma M_R}{\Sigma M_D} \qquad \text{(Equation 3.2)}$$

In practice, a factor of safety of 2 to 3 is commonly applied to resist overturning (Das, 2004).

In the case of the walls at Machu Picchu, the moment resisting overturning is generated by the weight of the wall itself. Resistance to toppling failures of individual units in the wall comes from the weight of the individual stones. The overturning moment is generated by the horizontal force of the soil and water behind the wall.

The forces generated by the weight of the wall and the lateral pressure from the soil are the forces at work in overturning today's state of the art retaining walls, as well. In the case of non-gravity cantilevered walls, the passive pressure generated in front of the wall also

contributes to the resisting moment; for anchored walls, the anchor contributes a portion of the resisting moment, too.

Figure 17. An overturning/toppling failure in a dry-stacked modular block wall. (Photo property of J. Boward)

3.1.3 Bearing Capacity

A wall's foundation subgrade must be checked for bearing capacity to be certain that the bearing capacity of the subgrade is sufficient to withstand the force exerted upon it by the retaining wall. The factor of safety for bearing capacity is the ratio of the ultimate bearing capacity of the soil to the pressure exerted at the base of the retaining wall's foundation. A factor of safety for bearing capacity equal to 3 is commonly used in practice (Das, 2004).

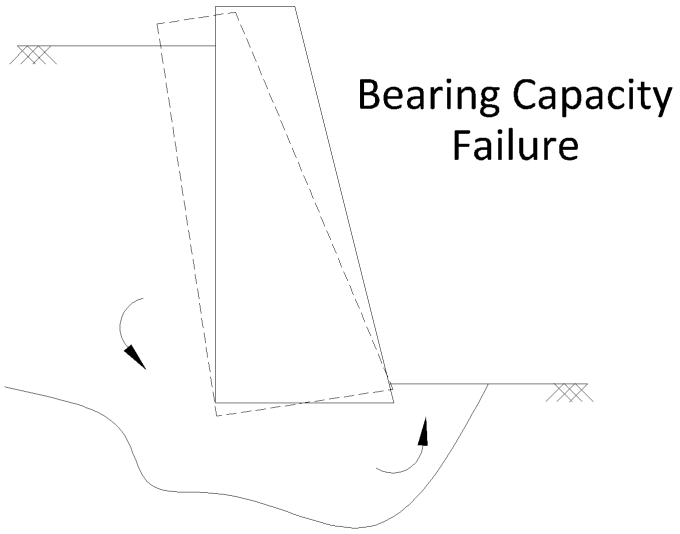

Figure 18. Illustration of bearing capacity failure.

3.2 MACHU PICCHU'S RETAINING WALLS

This section presents the results of a stability analysis of the retaining walls at Machu Picchu, including a simplified analysis to determine the walls' factor of safety against sliding and overturning.

The model used for the stability analysis is based on conservative information gleaned from published resources and assumed information. Because excavations are very rarely permitted at Machu Picchu, little is known about the backfill and foundation of the walls.

In the stability model, shown in Figure 19, the walls are seven feet high, made up of vertically-stacked granite blocks measuring one foot high by one foot wide by two and one-half feet deep. The angle of friction between the granite blocks is assumed to be 35 degrees and the unit weight of the blocks is assumed to be 160 pounds per cubic foot (Hoek and Bray, 1981).

As shown in Figure 13, the wall extends below grade at the front of the wall such that the wall analyzed herein sits atop a granite block.

The backfill is assumed to be a well-drained sand with no cohesion, an internal friction, φ, of 30 degrees, and a unit weight of 110 pounds per cubic foot, although Wright and Zegarra indicate that the backfill of the agricultural terraces is composed of several different layers, as shown in Figure 13. The simplified model used for this analysis assumes a single layer of backfill extending the entire height of the wall (rather than three distinct soil layers).

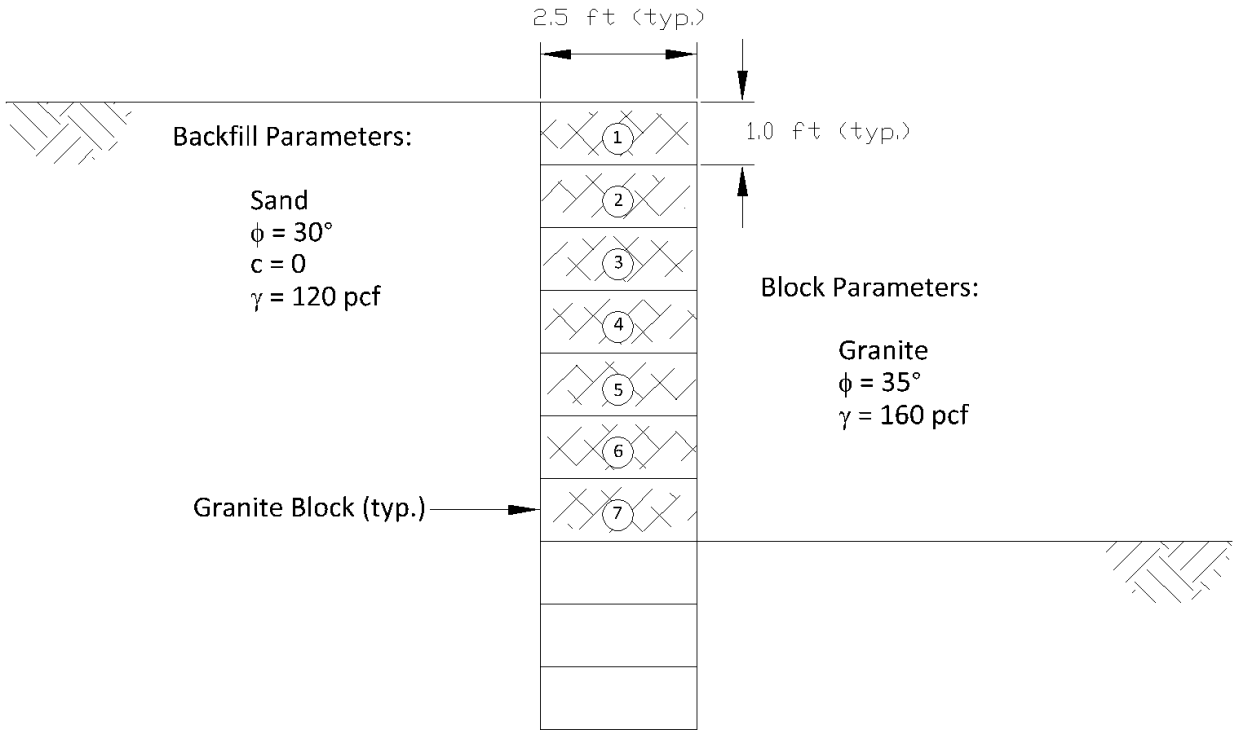

Figure 19. A simplified schematic drawing of the Incan walls used in the stability analysis.

The pressure generated behind the wall was calculated using Rankine theory. The backfill generated a pressure of 257 pounds per square foot, as indicated in Figure 20. No

hydrostatic pressure was included in this analysis; the Incan walls are well-drained, as indicated by Wright and Zegarra, so no hydrostatic pressure builds behind the walls.

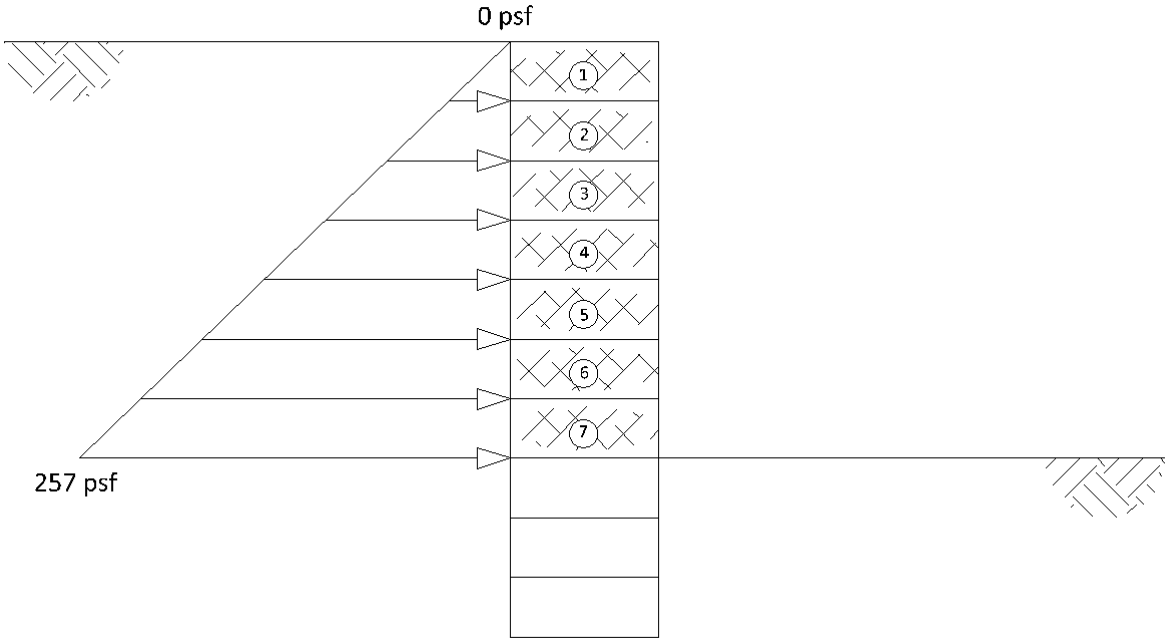

Figure 20. Active pressure generated behind the wall in the stability analysis.

3.2.1 Sliding

Two different sliding failure modes are possible in dry-stacked walls such as the model wall. The stones can slide with respect to one another (a “popout”-type failure where one block is pushed out from between two others), as illustrated in Figure 21, or the entire wall may slide with respect to the ground surface as if it were one monolithic unit, as shown in Figure 14. Both of these cases were evaluated for this stability analysis. Each case was also checked for seismic conditions, assuming a seismic coefficient of 0.15.

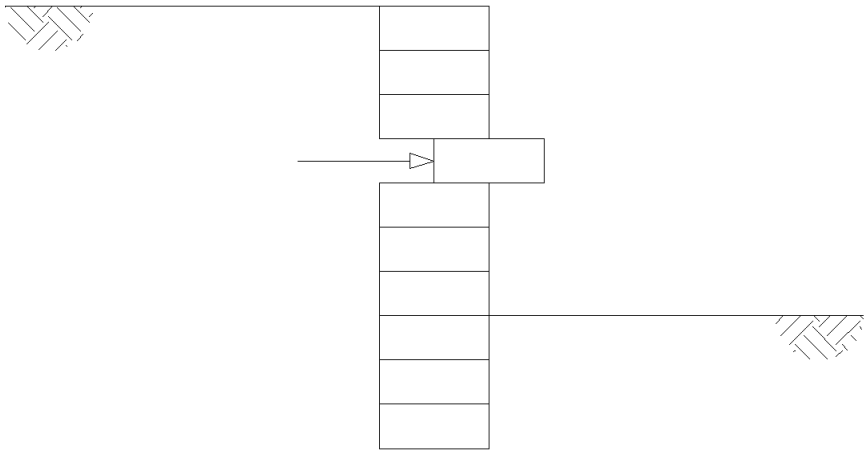

Figure 21. Illustration of a sliding "popout" failure.

In the case of stones sliding with respect to each other, three forces, shown in Figure 22, were at play: the force generated by the active pressure behind the particular stone; the friction force generated between the stone and its upper neighbor; and the friction force generated between the stone its lower neighbor. No passive earth pressure-generated forces are at work in this analysis as the wall does not truly extend below the ground surface. The factor of safety for each of the seven blocks making up the wall was calculated to be 12.5, and in the case of an earthquake, 10.8. Thus, when considering the stability of individual blocks with respect to one another, the retaining walls at Machu Picchu far exceed the typical modern minimum factor of safety against sliding.

The model wall was also analyzed for a monolithic sliding failure, assuming that the entire wall above a particular block slid forward along the base of that block. In this case, only two forces were at work: the force generated by the active soil pressure behind the wall and the friction force generated along the base of the block in question. Again, no passive earth pressure is generated in front of the wall. The calculated factors of safety are summarized in Table 1.

The factor of safety against sliding tends to decrease as the height of the failure increases, ranging from 12.0 (in a static situation with only the top block sliding) to 1.49 (in the case of an earthquake and all seven granite blocks sliding together). Again, these factors of safety are greater than or approximately equal to 1.5, usually the minimum factor of safety used in design today.

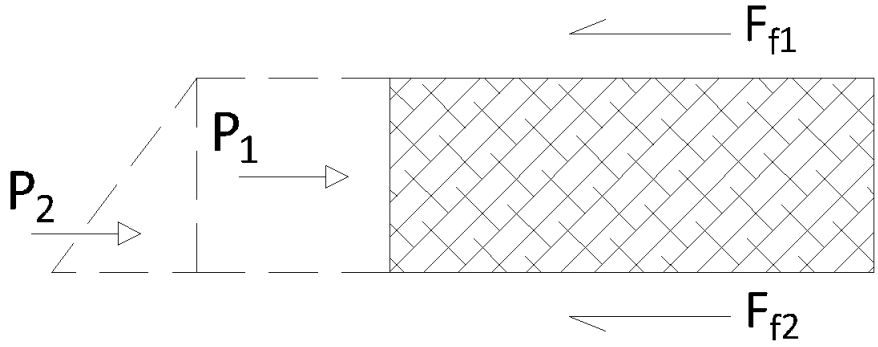

Figure 22. Forces acting on a single sliding block in the model.

Wright and Zegarra indicate that some of the walls were designed such that the individual stones have "top or bottom indentations that help them fit together in a nesting manner." While these indentations are not considered in this simplified stability analysis, it should increase the stability of the walls by contributing a greater resisting force, in addition to the friction force. As shown later in Section 5.1, the stones have a structural roughness which also contributes to the "interlocking" between individual wall units.

Table 1. Summary of sliding factors of safety for a monolithic sliding failure along the base of a particular block.

Block	FS_{static}	$FS_{seismic}$
1	12.0	10.4
2	5.98	5.20
3	3.99	3.47
4	2.99	2.60
5	2.39	2.08
6	1.99	1.73
7	1.71	1.49

3.2.2 Overturning

The model wall's factor of safety against overturning was also calculated in this analysis. Overturning about the front bottom corner of each block was considered, as shown typically in Figure 23. Two moments, each taken about the front bottom corner of the block in question, influence the factor of safety against overturning for this wall: the moment caused by the active soil pressure behind the wall and the resisting moment generated by the sum of the weights of the blocks above the point of overturning. Resistance is also affected by the fractal nature of the stone surfaces and size distribution of the stones, as will be discussed further in Section 4.0 and is not considered for the stability analysis.

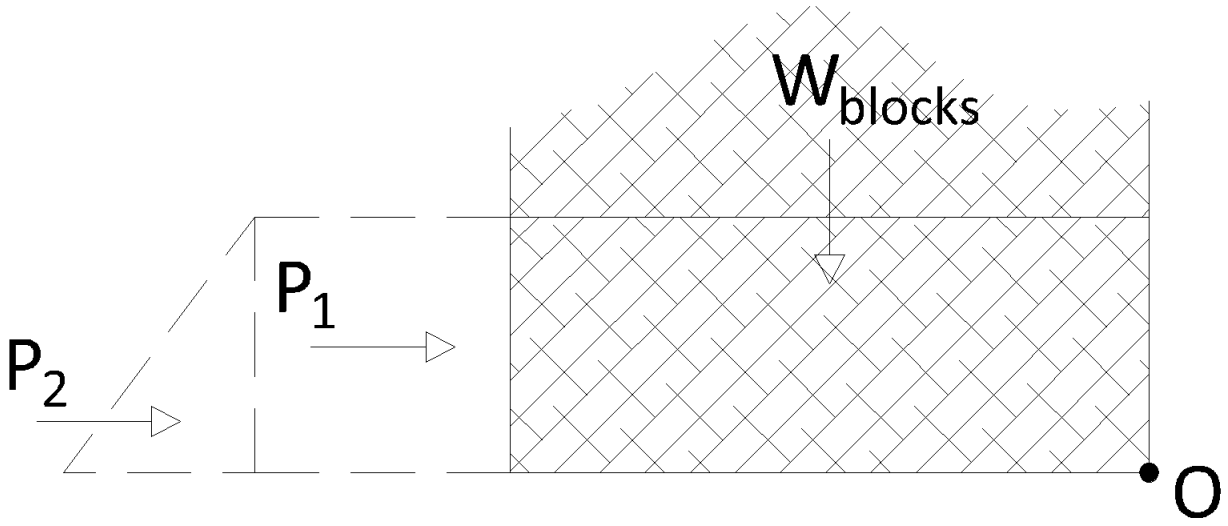

Figure 23. Illustration of forces acting on an overturning block in the model.

The factors of safety determined in this analysis and summarized above in Table 2, decreased with increasing wall height and ranged from 1.67 to 81.1. While the minimum factor of safety determined in this analysis, 1.67, is not as great as the typical modern-day factor of safety ranging from two to three, it is still greater than unity, indicating that the wall is indeed stable. Due to the generalized nature of this assessment, in reality the factor of safety for the Incan walls likely varies from the factors of safety determined herein.

Table 2. Summary of overturning factors of safety for a failure occurring at the base of the particular block.

Block	$FS_{overturning}$
1	81.8
2	20.5
3	9.01
4	5.11
5	3.27
6	2.27
7	1.67

3.2.3 Bearing Capacity

Although not quantitatively analyzed herein, Machu Picchu's retaining walls foundations appear to be adequately designed for bearing capacity. According to Wright and Zegarra, "to create a firm bedding," the Incas placed smaller stones in the bottom of the excavation where the walls were founded in soil and in the case of some much larger retaining walls, used very large stones for the foundation (or even built directly atop bedrock where possible).

4.0 FRACTAL ANALYSIS OF INCAN WALLS

4.1 FRACTALS

4.1.1 What is a Fractal?

In mathematicians' attempts to describe natural phenomena, difficult-to-describe natural objects are usually reduced to well-defined objects from Euclidean geometry. Planets can be seen as spheres, a blade of grass can be seen as a triangle, a mountain can be seen as a cone. Benoit Mandelbrot, often considered the father of fractal geometry, cautioned that "mountains are not cones, clouds are not spheres." Mandelbrot brought together many previously discovered mathematical peculiarities under the banner of "fractals" to describe these natural occurrences.

Fractals have been used to describe many irregular and seemingly random phenomena that cannot be fully explained with classical mathematical concepts: snowflakes; Brownian motion; coastlines; and other natural occurrences/processes. The topological dimension of an object comes from Euclidian geometry; a ball, a veil, and a thread can be modeled to be three-, two-, and one-dimensional, respectively (Mandelbrot, 1977).

Benoit Mandelbrot coined the term "fractal" in 1975 and defines it as "a set for which the Hausdorff-Betiscovitch dimension strictly exceeds the topological dimension," (Mandelbrot, 1977). Mandelbrot calls the Hausdorff-Betiscovitch dimension "the fractal dimension," denoted

as "*D*" because this dimension is often *fractional* (Baveye and Boast, 1998). Mandelbrot (1977) states that, "For every set *S*, there exists a real value *D* such that the d-measure [the topological dimension] is infinite for $d < D$ and vanishes for $d > D$." This D is the Hausdorff-Besicovitch dimension and the fractal dimension.

In a theoretical sense, fractals are part of a family of "mathematical monsters." These monster curves were discovered centuries ago by mathematicians (Baveye and Boast, 1998). An iterative approach is used to construct visual representations of the monster curves. An initiator (an equilateral triangle - three straight line segments - for the case of the Koch Snowflake, as shown in Figure 24) is drawn and then modified by a generator (in this case, a symmetrical peak constructed of two horizontal line segments and two angled line segments). The monster curve's construction is progressed by replacing each initiator with a generator, creating an increasingly complex shape. With each iteration, the curve begins to look more and more like a snowflake, as shown in Figure 24. As these monster curves were further developed over the years, they led to the visually stunning computer-generated "fractals" we see today.

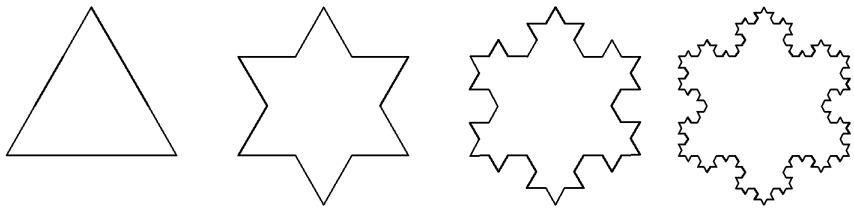

Figure 24. Generation of the Koch Snowflake through four iterations.

A fractal can be described visually as something that is self-similar and scaling. Fractals are roughly identical at any scale, small or large (Mandelbrot, 1982); for example, the Koch Snowflake pictured above shows an equilateral triangle at four different scales (the triangle

becomes smaller with each iteration). A tree can be considered fractal. Looking at an entire tree is roughly the same as looking at one branch of that tree but with a different scale. They each have a main stem (the trunk in the case of a whole tree or a limb in the case of the branch). Smaller limbs, branches, and twigs split off from the main stem. From these smaller limbs, even smaller limbs divide, and so on. As one zooms into the tree, one sees the same general pattern as that displayed by the entire tree, as shown in Figure 25. This concept can be applied to many natural objects: consider a fern, a head of cauliflower, a mountain, a network of rivers and streams, or the human circulatory system; they are all fractals.

Figure 25. Trees are one example of a naturally-occurring fractal pattern.

4.1.2 Fractals and Roughness

Hyslip and Vallejo (1997) showed that the roughness of a population of fractal shapes can be quantified using the area-perimeter method. The linear extent of a geometric pattern can be represented by its perimeter (*P*), the square-root of its area ($A^{1/2}$), or the cube-root of its volume ($V^{1/3}$). The ratio of any two of a pattern's linear extents gives a constant that is specific to that pattern. Consider a circle with a radius, r:

$$P = 2\pi r \qquad \text{(Equation 4.1)}$$

$$A = \pi r^2 \qquad \text{(Equation 4.2)}$$

Taking the ratio of the linear extents of the circle gives:

$$\frac{P}{A^{1/2}} = \frac{2\pi r}{(\pi r^2)^{1/2}} = (4\pi)^{1/2} = c_c \qquad \text{(Equation 4.3)}$$

It can be seen that for any circle, the relationship in Equation 4.3 holds true. The ratio of the linear extents for other geometric patterns yields the pattern's unique constant.

A quantitative measure of a geometrically similar population of fractal shapes can be obtained through the ratio of linear extents for that population (Mandelbrot, 1983 as cited by Hyslip and Vallejo, 1997). Mandelbrot proposed that the "ratio of linear extents" is fractal for fractal patterns and proposed that:

$$c = \frac{P^{1/D_R}}{A^{1/2}} \qquad \text{(Equation 4.4)}$$

where c is a constant and D_R is the value of the roughness fractal dimension for the population of fractal patterns. A log-log plot of P vs. A for each individual object in the population yields a straight line with a slope, m, related to the fractal dimension by:

$$D_R = \frac{2}{m} \qquad \text{(Equation 4.5)}$$

This type of analysis, the area-perimeter method, quantifies the roughness of a population of similar geometric patterns. The roughness quantity can be representative of either the structural or the textural characteristics of the population, depending on the level of scrutiny (Hyslip and Vallejo, 1997). At a low resolution, an object's general structure is quantified; at a high resolution, an object's textural characteristics are quantified.

4.1.3 Fractals and Distribution/Fragmentation

Populations exhibiting fractal characteristics, commonly called probabilistic fractals, can exhibit a power law relationship as a result of their fractal geometry (Baveye and Boast, 1998). The Pareto or power law distribution, originally illustrating the distribution of income in a population, is given by the equation:

$$N = Ax^{-\alpha} \qquad \text{(Equation 4.6)}$$

where N is the number of persons having income $\geq x$. Plotting N as a function of x results in a distribution with a long right tail.

This concept can be extended to perimeter-area plots. As demonstrated in Korvin (1992), J. Korcak (1940) found during his analysis of the perimeter and area of islands that the distribution of a population geographic objects follows a pareto distribution and proposed the following equation, Kocak's Law, where *k* and *b* are constants and *A* represents area:

$$\Pr(A > a) = ka^{-b} \qquad \text{(Equation 4.7)}$$

Mandelbrot, realizing that this distribution was a result of fractal fragmentation, applied Korcak's Law to fractals. He suggested that *b* in Equation 4.7 is equal to the fragmentation fractal dimension, D_F, and developed the following equation:

$$N(R > r) = kr^{-D_F} \qquad \text{(Equation 4.8)}$$

Where *N(R>r)* is the total number of particles with a linear dimension *R* greater than a given size *r* and *k* is a constant as in Equation 4.7. A log-log plot of N(R>r) will genearate a straight line with a slope m where:

$$D_F = -2m \qquad \text{(Equation 4.9)}$$

Equations 4.8 and 4.9 are based on the linear dimension of an object (radius, perimeter, diameter, etc.). Relating these relationships to area, whose linear extent is the square-root of area, gives:

$$N(A > a) = ka^{-D_F/2} \qquad \text{(Equation 4.10)}$$

$$D_F = -2m \qquad \text{(Equation 4.11)}$$

Thus, a log-log plot of $N(A>a)$ vs. a will generate a straight line with a slope equal to $-D_F/2$.

It should be noted that D_F differs from the previously described D_R and is not representative of the roughness or shape of a specific population of objects, but rather a measure of the *distribution* of that population's specific traits (area, in the case of Equations 4.10 and 4.11).

4.1.4 Fractal Behavior of the Retaining Walls at Machu Picchu

In his 1977 publication's chapter entitled "How Long Is the Coast of Britain?" Mandelbrot describes how the concept of fractals and the fractal dimension can be applied to coastlines and islands. The rocks that make up the retaining walls at Machu Picchu are analogous to islands. By visualizing the walls as two-dimensional (when viewing the front face of the wall), the irregular outline of the individual rock faces can be equated to that of an island, as shown in Figure 26.

The coastline of an island and the perimeter of a rock face demonstrate fractal properties. At any scale, one can see the boundary between the object and its surroundings: water in the case of an island, and the other stones in the case of the retaining walls. As one zooms in closer on the object's boundary line (demonstrated in Figure 27), more and more asperities become visible, and the boundary line is just as chaotic as it was when observing the entire object. This erratic boundary line cannot be easily described by Euclidean geometry; but the self-similar, scaling behavior of the boundary line can be described as a fractal. Not only are the boundaries of the

individual stones fractal, but the size distribution of the stones forming each wall has a fractal dimension, as discussed in Section 5.2.

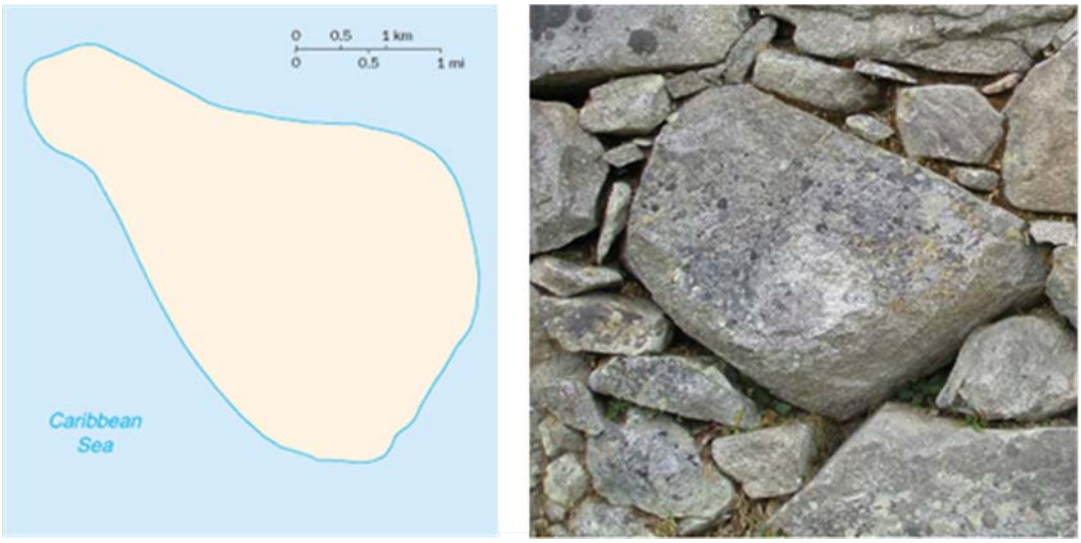

Figure 26. Comparing an island (left) to a stone (right).

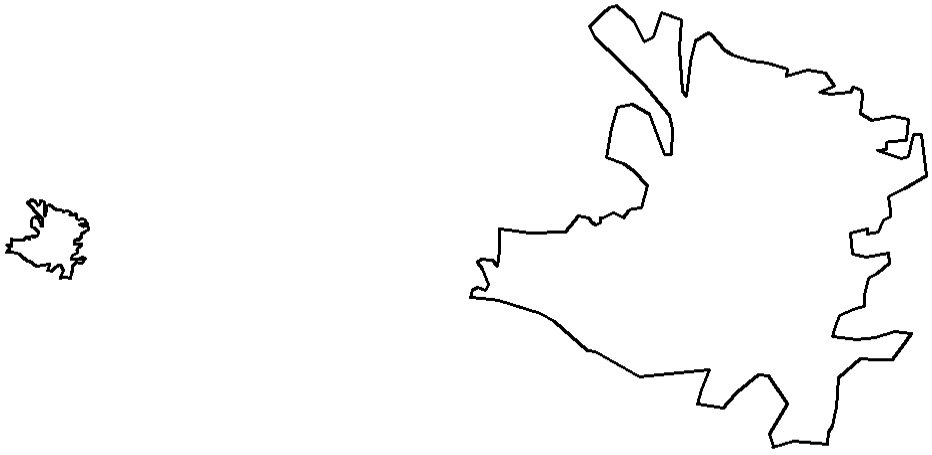

Figure 27. An island shown at two different scales.

4.2 FORCE CHAINS

Vallejo et al. (2005) investigated the crushing of granular materials and found that granular materials, when subjected to various loads, form force chains through which the load is carried. Force chains form when the applied load is passed through the contacts between granular materials. Using the discrete element method in a computer model, they found that the size (thickness) of the force chains varied proportionately to the applied load and that the distribution of force chains in the matrix is fractal.

The retaining walls at Machu Picchu may be considered analogous to the model used by Vallejo. The walls are a matrix of granular particles (albeit on a much larger scale than that investigated by Vallejo) subjected to vertical loads imposed the particles' self weight.

4.3 FRACTAL ANALYSIS OF THE WALLS AT MACHU PICCHU

4.3.1 Fractal Analysis Using Digitized Photos

Figure 33 through Figure 37 are photos, taken by L.E. Vallejo in 2007, showing the five walls subject to analysis in this study. Figure 33 through Figure 36 show four retaining walls, while Figure 37 shows a stone dwelling wall at Machu Picchu.

Figure 28. Wall 1 (Photo property of L.E. Vallejo)

Figure 29. Wall 2 (Photo property of L.E. Vallejo)

Figure 30. Wall 3 (Photo property of L.E. Vallejo)

Figure 31. Wall 4 (Photo property of L.E. Vallejo)

Figure 32. Wall 5 (Photo property of L.E. Vallejo)

These five photos were digitized, as shown below in Figure 33 through Figure 37, using AutoCAD 2007 software by AutoDesk, Inc., on a personal computer. Each individual stone making up the walls was outlined by visual estimation of the boundary and modeled as a polygon in the program. The area and perimeter of each individual polygon representing a rock face were determined by the software and recorded for use in the fractal analysis, as discussed in Chapter 5.0.

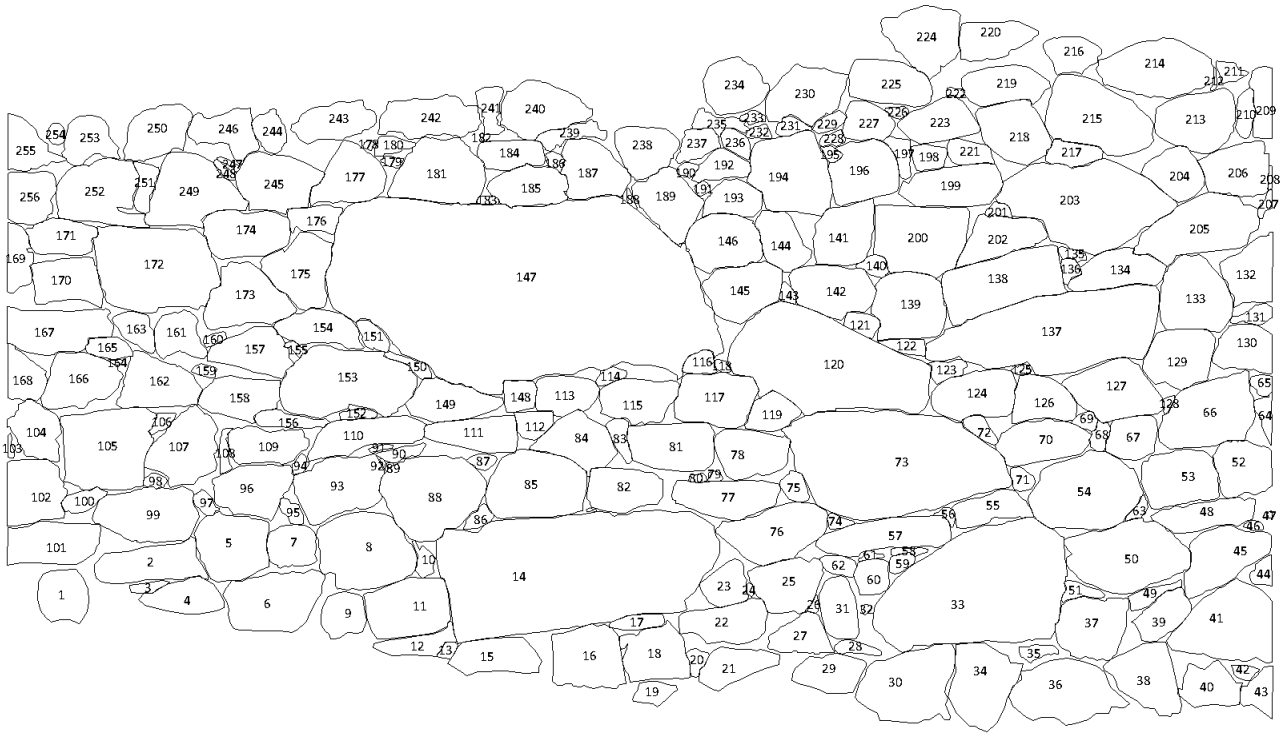

Figure 33. Wall 1 - Digitized

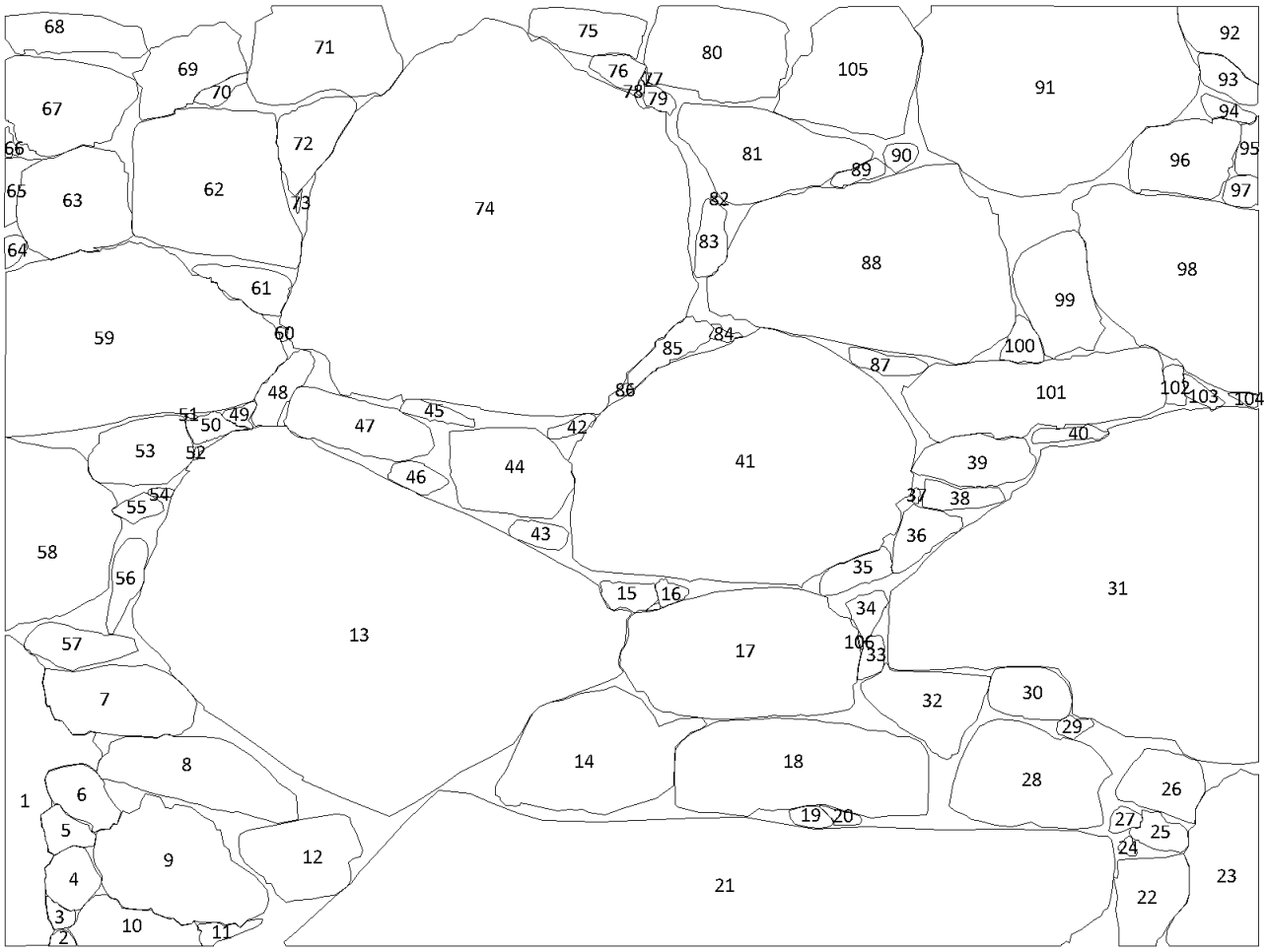

Figure 34. Wall 2 - Digitized

Figure 35. Wall 3 - Digitized

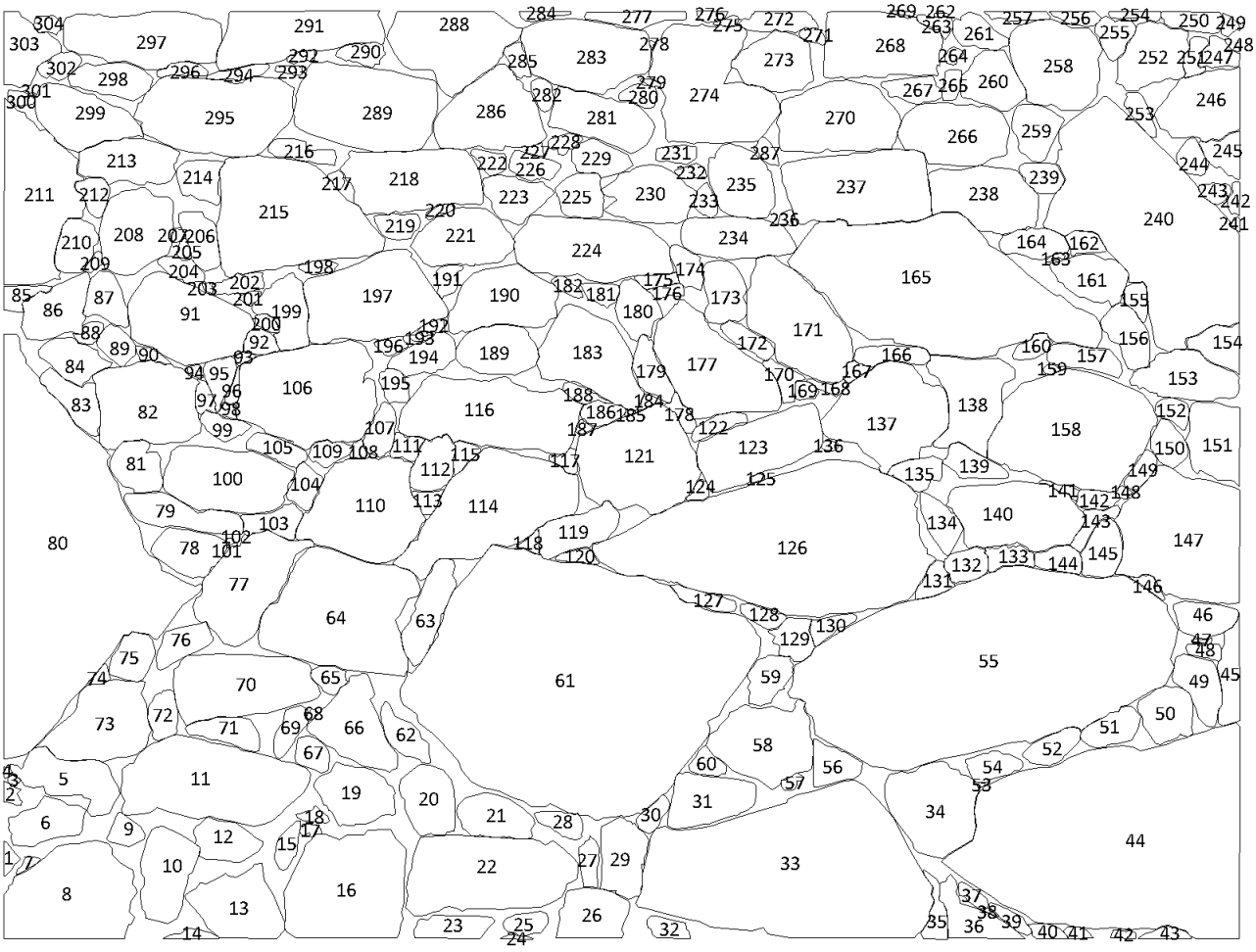

Figure 36. Wall 4 - Digitized

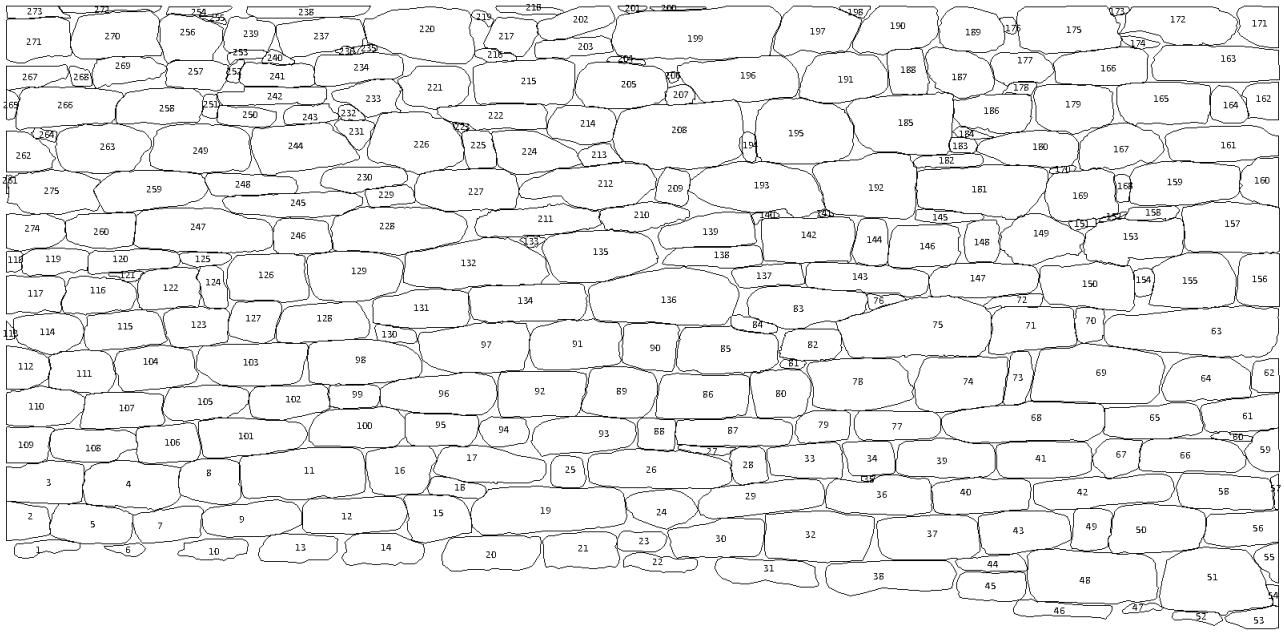

Figure 37. Wall 5 - Digitized

5.0 ANALYSIS AND RESULTS

5.1 ROUGHNESS OF THE INCAN WALLS

Each of the five wall photographs were digitized and analyzed as described in Chapter 4.0. For each wall, the corresponding perimeter (*P*) and area (*A*) for each individual stone making up the particular wall were plotted on a log-log graph, employing the relationships introduced in Section 4.1. Stones along the "perimeter" of the photo were eliminated from the analysis for the four retaining walls and the middle one-third of stones making up the house wall were examined, as many of the stones along the edges of the photo were cut-off by the camera and were not representative of the actual size and dimension of the stones making up the wall. Least squares linear regression was used to determine the line of best fit through all of the remaining data points. Figure 38 through Figure 42 show the five perimeter-area (*P* vs. *A*) plots generated for the walls.

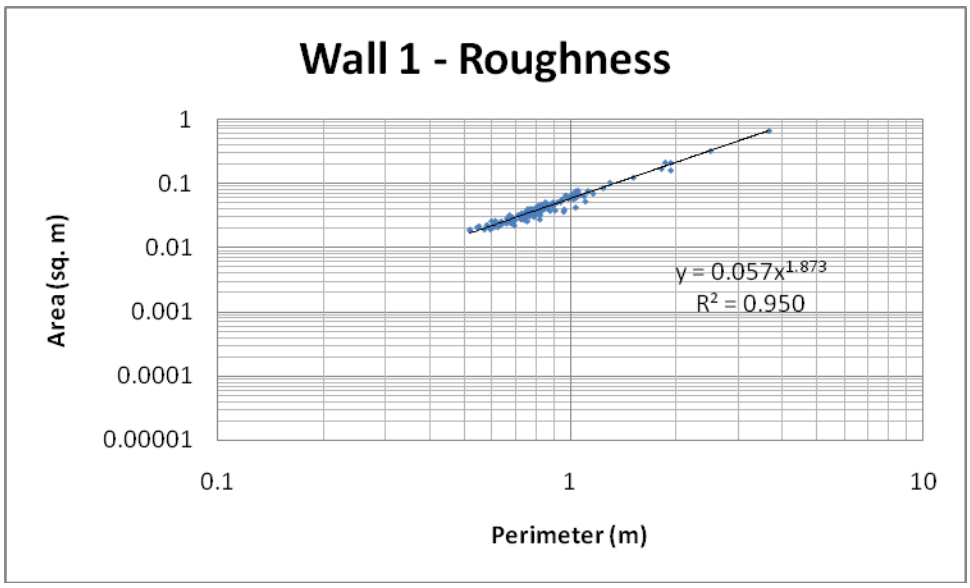

Figure 38. Wall 1 – *P* vs. *A*

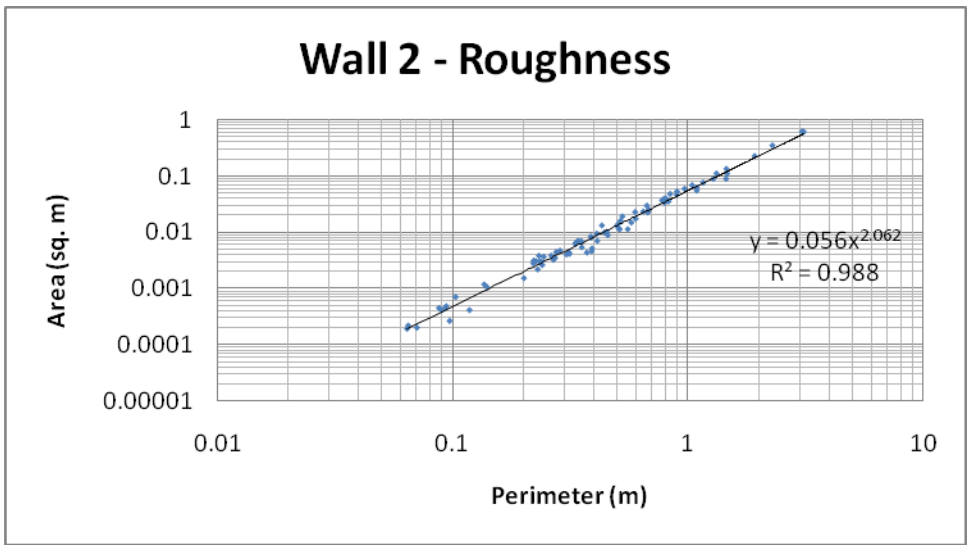

Figure 39. Wall 2 – *P* vs. *A*

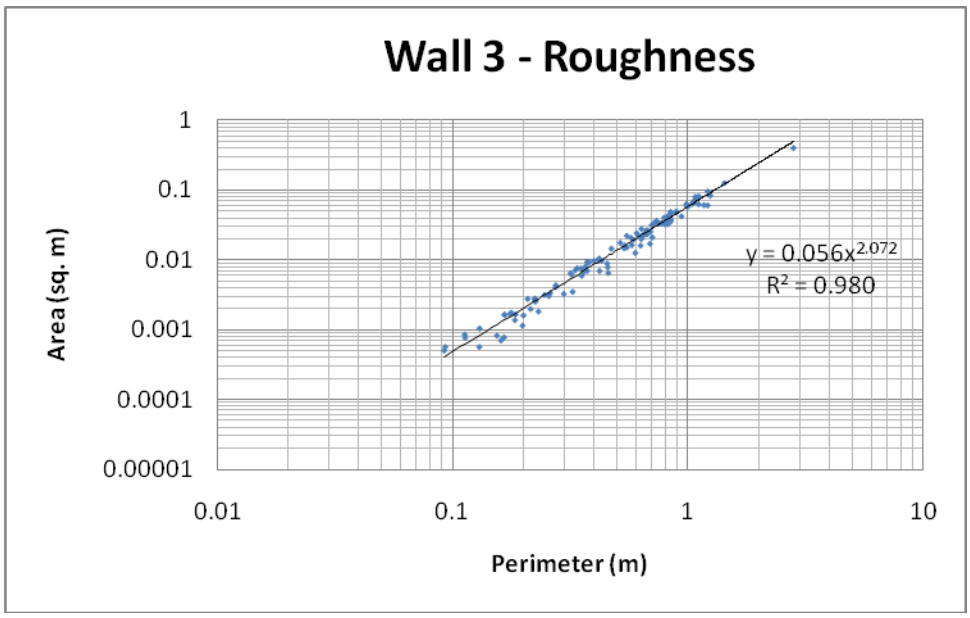

Figure 40. Wall 3 – *P* vs. *A*

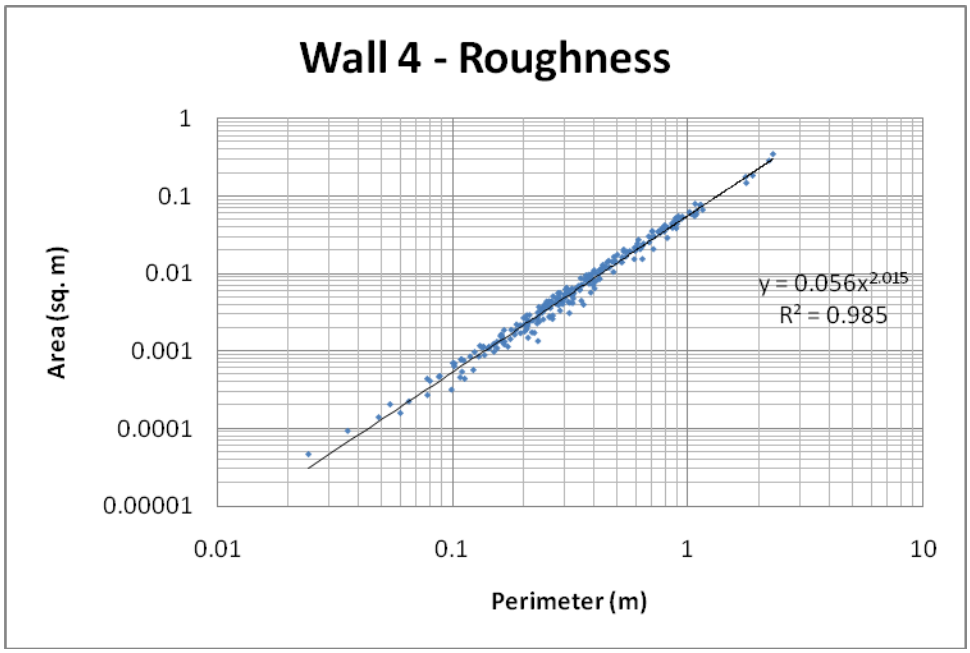

Figure 41. Wall 4 – *P* vs. *A*

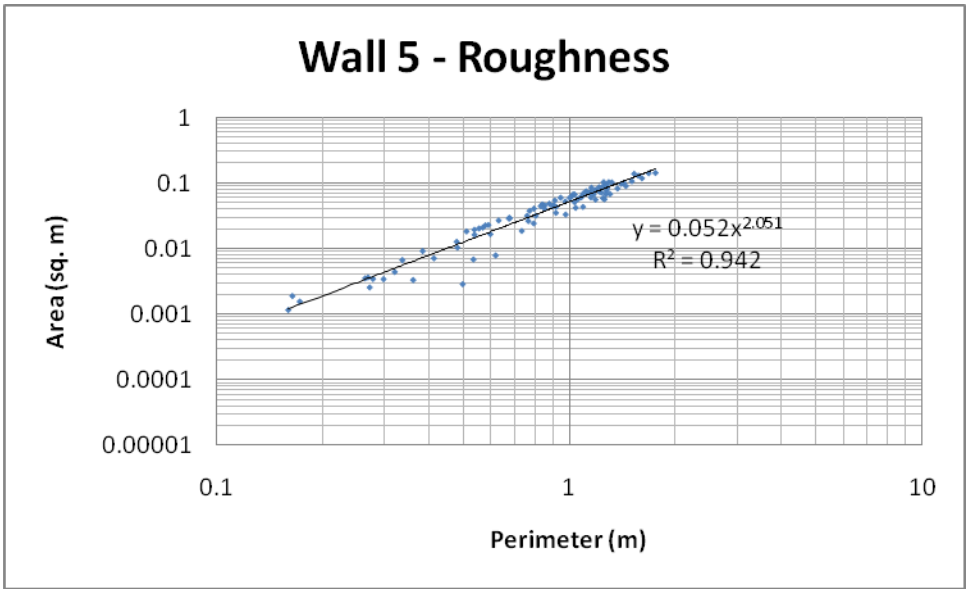

Figure 42. Wall 5 - *P* vs. *A*

Table 3. Values of D_R and correlation coefficients for the walls

	D_R	**R^2**
Wall 1	1.07	0.950
Wall 2	0.970	0.988
Wall 3	0.965	0.980
Wall 4	0.993	0.985
Wall 5	0.975	0.942

As shown by the *P* vs. *A* plots above, the data fits a power-law distribution as discussed in Chapter 4.1.2, with a correlation coefficient ranging from 0.942 to 0.988. The roughness fractal dimension for the five walls examined in this study ranged from 0.965 to 1.07. The average fractal roughness dimension for the walls is 0.995. The range in roughness for the walls

indicates that the stones making up Wall 3 are the smoothest, while those making up Wall 1 are the roughest.

Wall 2, Wall 3, Wall 4, and Wall 5 all appear to have a roughness dimension less than one based upon the results of the least squares regression analysis. In fractal geometry, as in Euclidean geometry, a dimension equal to zero represents a single point and a dimension of unity represents a solid line. A dimension between zero and unity, possible in the realm of fractal geometry, represents a broken line. Thus, the minimum dimension of any of the stones making up the walls at Machu Picchu should be one (they are each represented by an unbroken line encompassing the area of the stone). Although the perimeters of all of the rocks modeled in this analysis are actually solid lines, due to the fact that the line of best fit generated by the least squares regression analysis depends upon values of the entire population, the slope of the line of best fit can be skewed to give a misleading roughness dimension.

Because the level of scrutiny of the stones' perimeters is relatively low (a low level of magnification was used to determine the perimeter), the roughness dimensions determined in this study relate to the structural characteristics of the stones rather than their textural characteristics, as described in Chapter 4.1.2. Roughness is important in the Incan walls because of its relationship to friction. The rougher a surface, the more asperities it has. It takes more energy for these asperities to push past one another (Lambe and Whitman, 1969), and hence a greater frictional resistance is developed between the individual rocks making up the wall, mitigating the risk of a "popout"-type failure. This is true on both a microscopic and macroscopic scale. The roughness dimension determined in this study is related to the structure rather than texture of the stones. The macroscopic asperities of the stones' surfaces help "interlock" the units making up the wall, adding additional strength to the wall, not considered in Section 3.2

5.2 DISTRIBUTION/FRAGMENTATION OF THE INCAN WALLS

As described in Chapter 4.3.1, the five wall photographs were digitized and each stone's perimeter and area were recorded for use in the fractal analysis described herein. To analyze the size distribution of stones making up the walls, a log-log plot of the area versus the number of stones with an area greater than a specified area (*a* vs. *N(A>a)*), in accordance with the theory described in Chapter 4.1.3. Again, stones along the "perimeter" of the photo were eliminated from the analysis for the four retaining walls and the middle one-third of stones making up the house wall were examined. Least squares linear regression was used to determine the line of best fit through all of the remaining data points.

As seen in Figure 43 through Figure 47, the plot of *a* vs. *N(A>a)* for each of the walls does not yield a straight-line correlation between all points, as did the *P* vs. *A* plots in Chapter 5.1. This difference is quantified by the significantly lower correlation coefficients listed in Table 4.

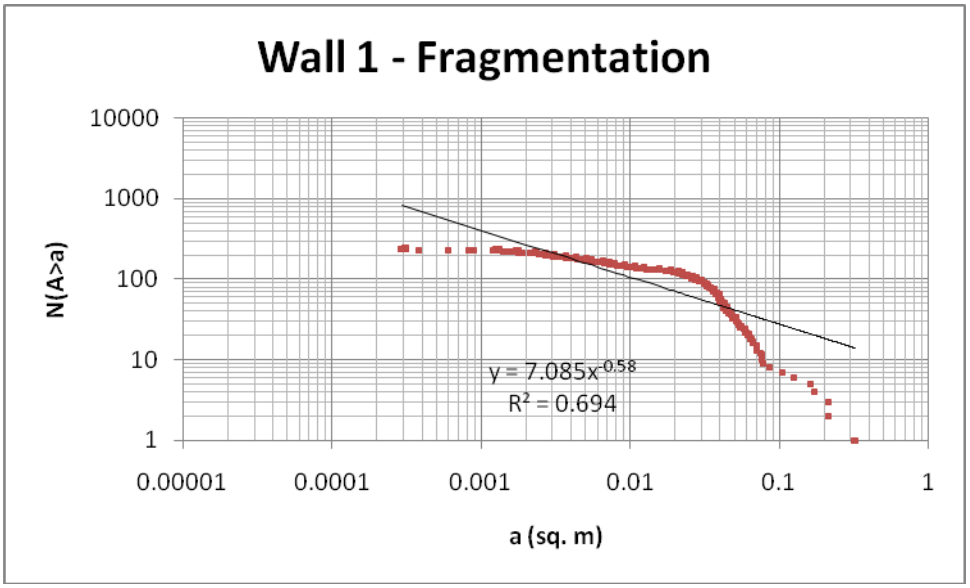

Figure 43. Wall 1 - *a* vs. *N(A>a)*

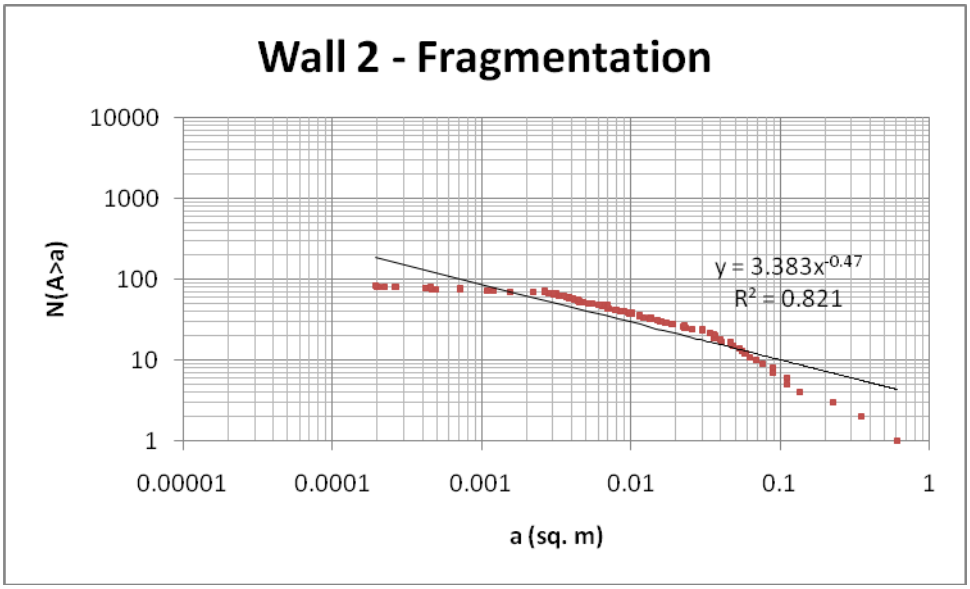

Figure 44. Wall 2 - *a* vs. *N(A>a)*

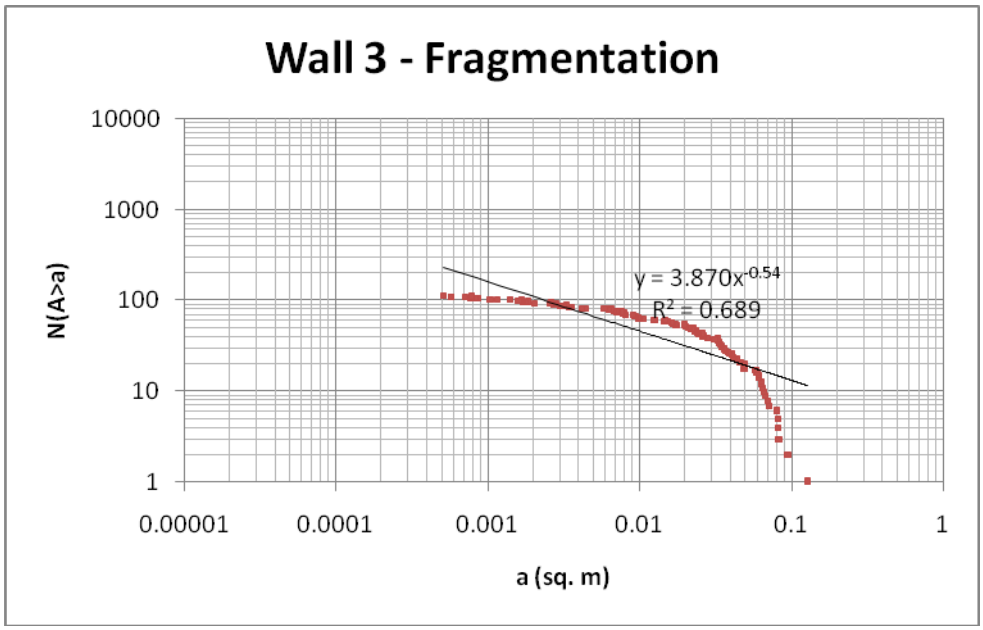

Figure 45. Wall 3 - *a* vs. *N(A>a)*

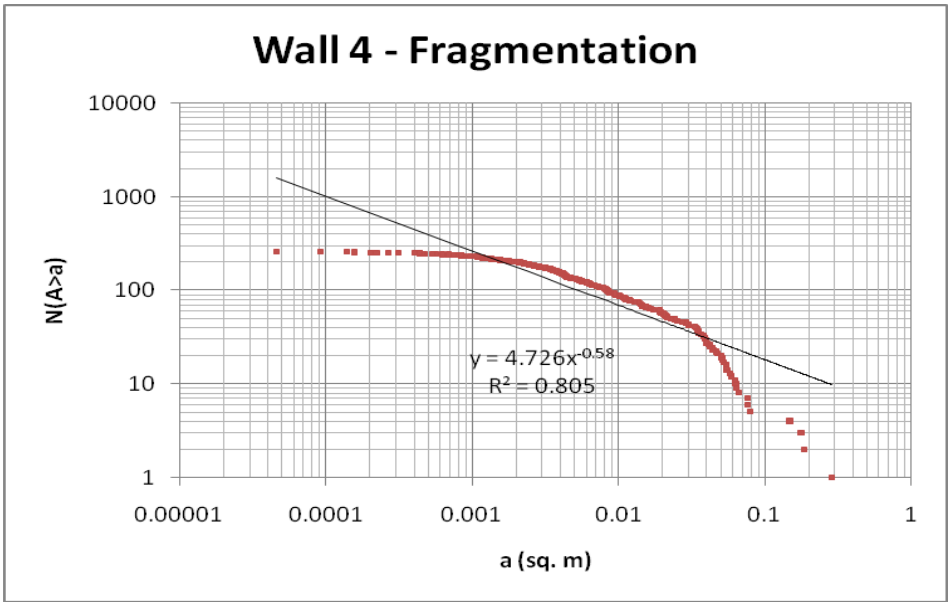

Figure 46. Wall 4 - *a* vs. *N(A>a)*

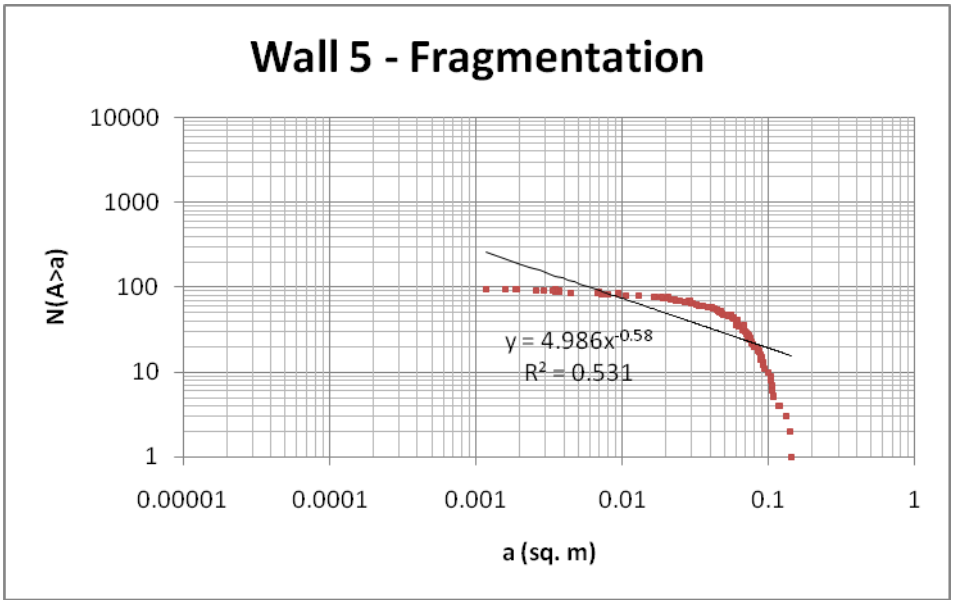

Figure 47. Wall 5 - *a* vs. *N(A>a)*

Table 4. Values of D_F and correlation coefficients for the walls.

	D_F	R^2
Wall 1	1.16	0.694
Wall 2	0.94	0.821
Wall 3	1.08	0.689
Wall 4	1.16	0.805
Wall 5	1.16	0.531

The fractal fragmentation dimensions of the walls range from 0.94 to 1.16. Wall 5, whose blocks have a more "uniform" appearance, does not reflect this visual difference in the "average" dimension obtained through these plots, although the curve does exhibit more of a "boomerang" shape than the other graphs do. The differing composition of Wall 5 is also reflected in its relatively low correlation coefficient. Walls 1, 4, and 5 each have a fractal dimension of 1.16, however the correlation coefficients, as well as a visual inspection of the data, do not indicate a very good fit between the trend line and the actual data points. Although each graph does not exhibit a *single* straight line correlation between data points, one could imagine that the data points on these graphs form several distinct, connected straight-line segments. The same graphs of *a* vs. *N(A>a)* are shown below in Figure 48 through Figure 52. These distinct straight-line correlations indicate that the stones making up the walls are fractal over at least three size ranges (Figure 49) and as many as five size ranges (Figure 52).

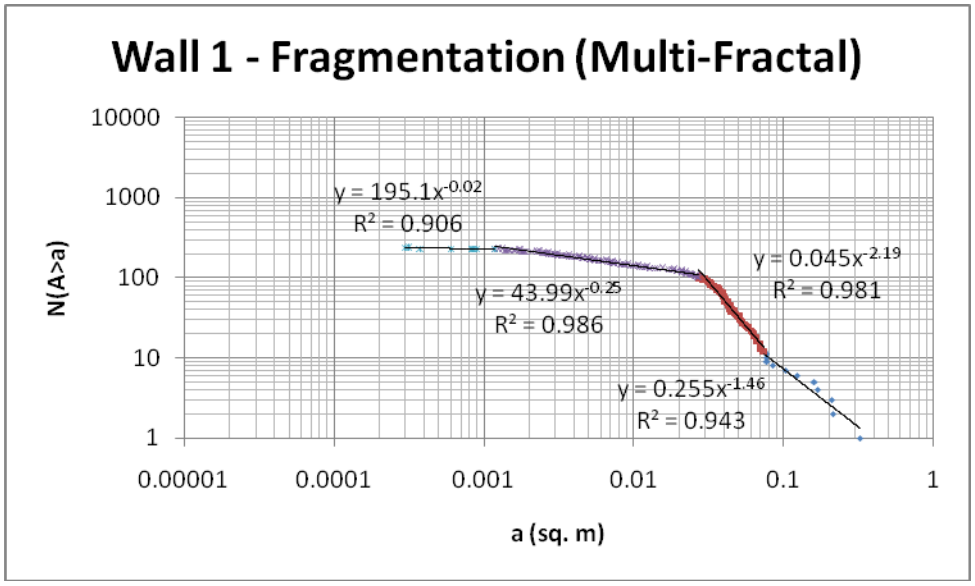

Figure 48. Wall 1 – Multi-fractal dimensions

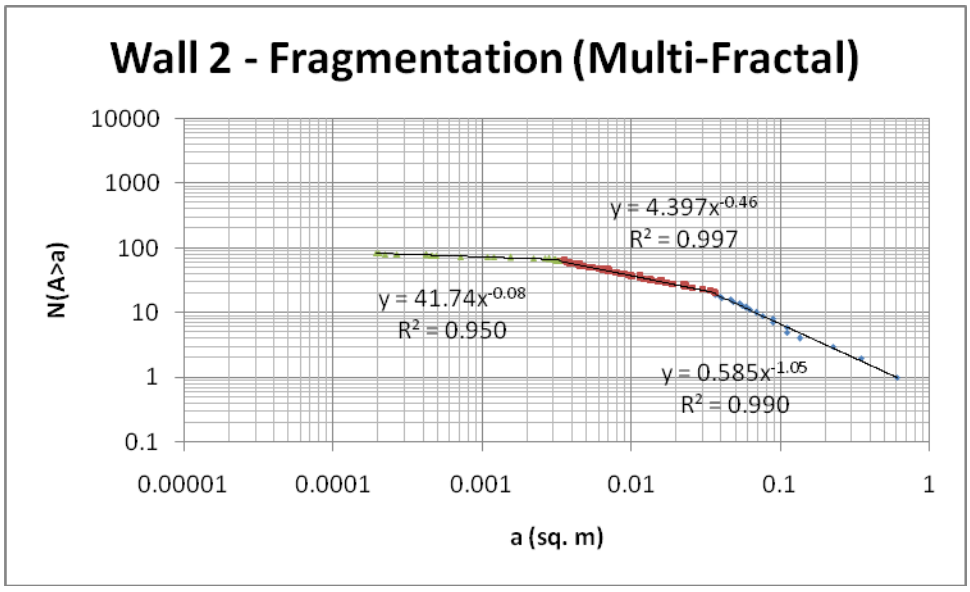

Figure 49. Wall 2 - Multi-fractal dimensions

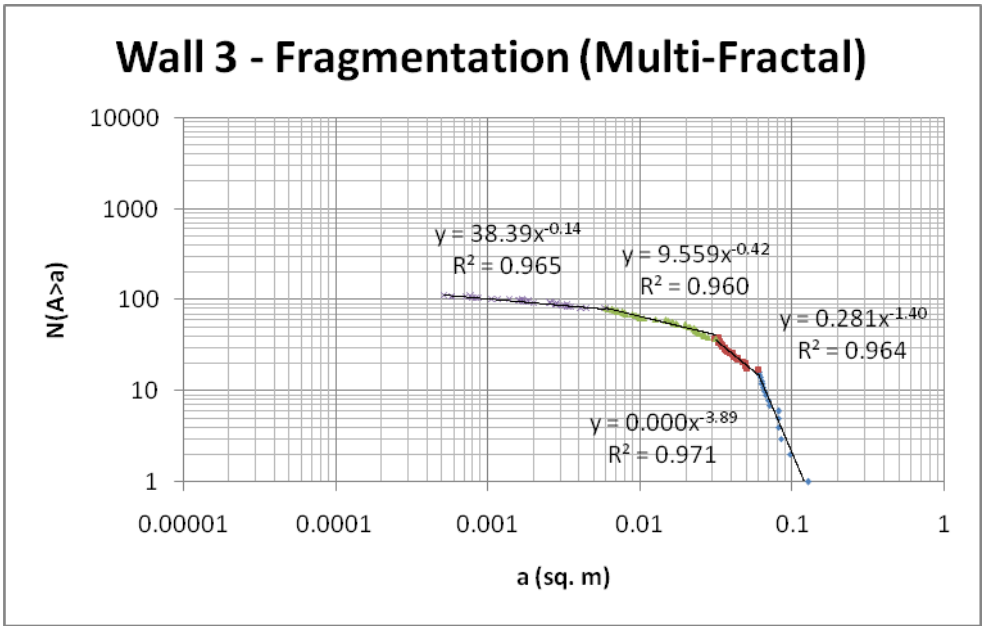

Figure 50. Wall 3 - Multi-fractal dimensions

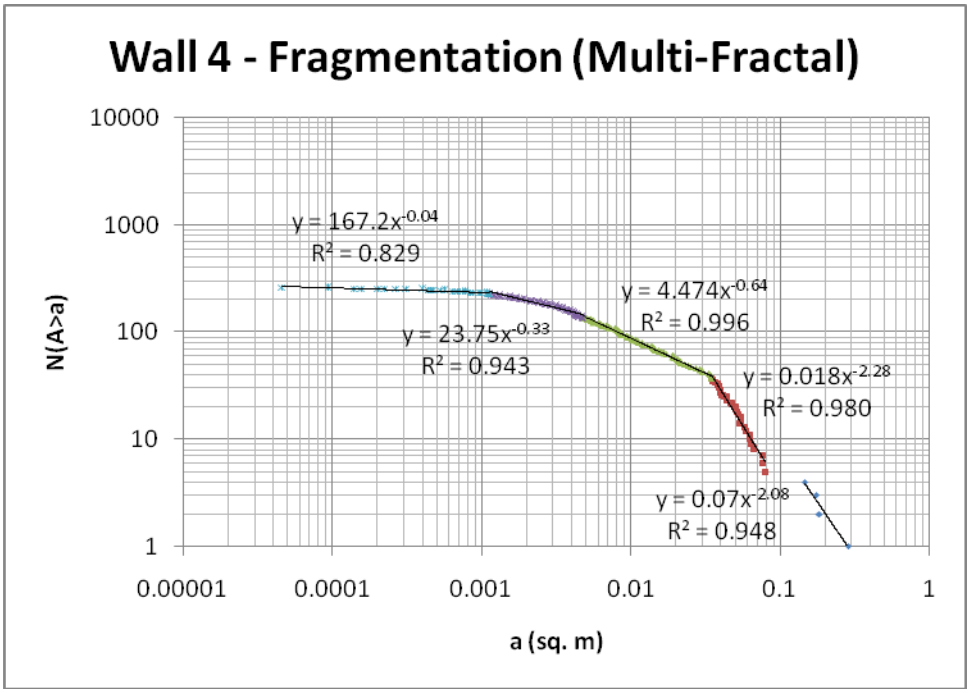

Figure 51. Wall 4 - Multi-fractal dimensions

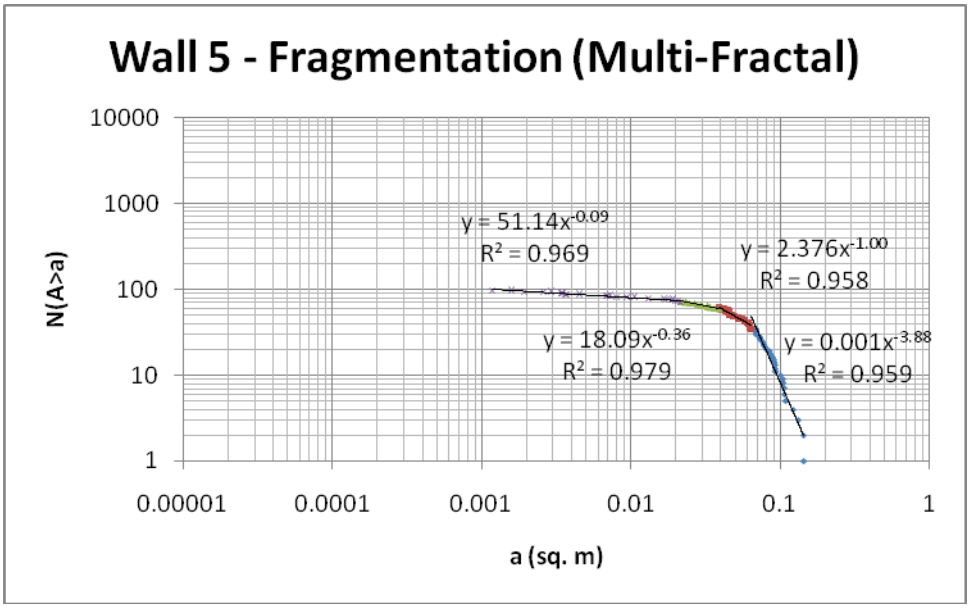

Figure 52. Wall 5 - Multi-fractal dimensions

Table 5. Comparison of multi-fractal D_F for all walls.

	Wall 1	**Wall 2**	**Wall 3**	**Wall 4**	**Wall 5**
D_{F1}	*0.040*	*0.160*	*0.280*	*0.080*	*0.180*
R^2_1	0.906	0.950	0.965	0.829	0.969
a_{1min} (m^2)	0.000297	0.000195	0.000511	0.0000465	0.00118
a_{1max} (m^2)	0.00119	0.00327	0.00598	0.00113	0.0215
D_{F2}	*0.500*	*0.920*	*0.840*	*0.660*	*0.720*
R^2_2	0.986	0.997	0.960	0.943	0.979
a_{2min} (m^2)	0.0019	0.00327	0.00598	0.00113	0.0215
a_{2max} (m^2)	0.0272	0.0366	0.0318	.00481	0.0386
D_{F3}	*4.38*	*2.10*	*2.80*	*1.28*	*2.00*
R^2_3	0.981	0.990	0.964	0.996	0.958
a_{3min} (m^2)	0.0272	.0366	0.0318	0.00481	0.0386
a_{3max} (m^2)	0.0751	0.608	0.0594	0.0346	0.0634
D_{F4}	*2.92*	-	*7.78*	*4.56*	*7.76*
R^2_4	0.943	-	0.971	0.980	0.959
a_{4min} (m^2)	0.0751	-	.0594	0.0346	0.0634
a_{4max} (m^2)	0.325	-	0.127	0.0789	0.145
D_{F5}	-	-	-	4.16	-
R^2_5	-	-	-	0.948	-
a_{5min} (m^2)	-	-	-	0.0789	-
a_{5max} (m^2)	-	-	-	0.284	-

Table 5 summarizes the fractal dimensions, correlation coefficients, and size range (in terms of area) that each of these straight-line relationships encompasses. All of the walls demonstrate similar ranges of fractal sizes.

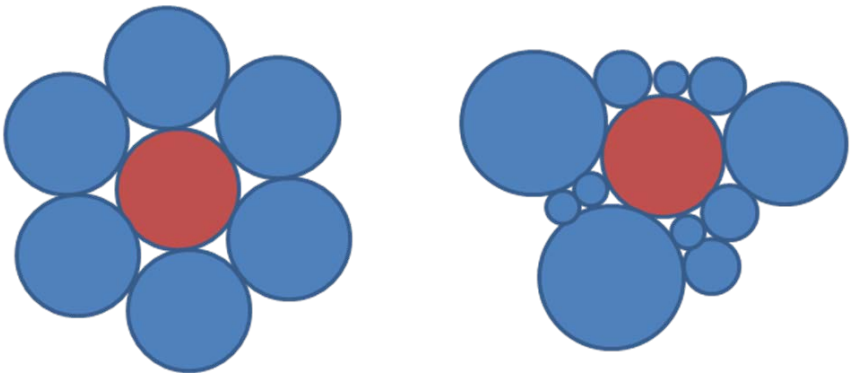

Figure 53. Packing of uniform size stones (left) and packing of various sizes of stones (right).

The fractal size distribution of the stones making up the walls is important to wall stability because a range of stone sizes allows more efficient packing of the stones around each other and thus produces more points of contact between the stones, as shown in Figure 53. The uniform-sized circles have only six points of contact with the purple circle, whereas the mixed-sized circles have nine points of contact with the purple circle. Greater contacting has an effect on how load is distributed throughout the walls, as will be demonstrated via laboratory analogy in Section 5.3.

5.3 FORCE CHAINS IN THE INCAN WALLS

The direct shear apparatus, shown in Figure 54, was used to simulate the effects of gravity on a "wall" composed of wooden dowels, approximately three centimeters in length to match the

depth of the apparatus, of various diameters (five, seven, and nine millimeters). As shown in the figures throughout this section, varying size distributions of dowels were placed in the direct shear apparatus and a normal load was applied to the dowels. The normal load simulates gravity and surcharge loads experienced by the individual elements of the wall, with individual wall elements represented by the dowels. Each of these distributions was photographed and selected distributions were digitized using AutoCAD 2007 software. The geometric properties of the resulting digitized images were used to determine the fractal roughness and fragmentation dimensions of the selected size distributions.

Yoshido (2004) found that when normal and shear loads of varying magnitudes were applied to an arrangement of dowels, force chains formed within the dowel matrix. Some of the dowels were not engaged by the force chains. The dowels which were not engaged appeared loose and were easily removed from the matrix. Upon removing these loose dowels, it became apparent that the dowels engaged by the force chain form an arch. The load is transmitted through the dowels making up the arch, and the loose dowels can be removed with no consequence to the remaining dowels in the matrix.

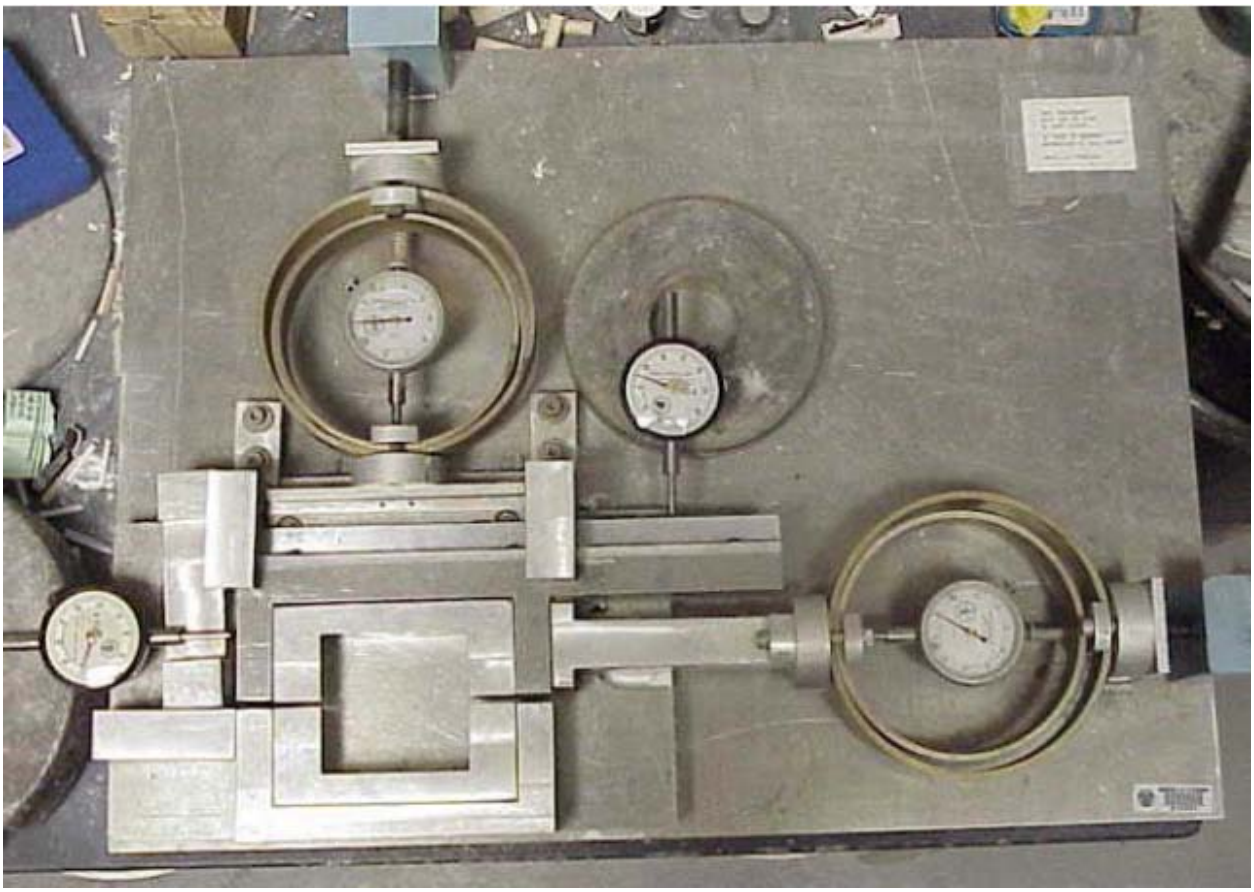

Figure 54. Direct Shear Apparatus (Vallejo, 1991)

The goal of the experiment detailed below, modeled after Yoshido's, is to show that in a "well-graded" distribution of units (in this case, dowels) making up a wall, more of the units will be engaged in the force chains leading to fewer "pop-outs" and greater overall stability for the wall. While pop-outs will not adversely affect the vertical load-bearing characteristics of such a wall, it will affect the lateral resistance of the wall. With one stone not engaged in providing lateral resistance, it will be pushed out of the wall by the lateral force of the soil. The arching effects of the soil will distribute the lateral load to the nearby stones remaining in place. An

increase in the load that they see may cause them to fail, leading to a chain reaction that causes failure in the entire wall.

The first test involved 67 seven-millimeter diameter round dowels. As shown in Figure 55, the dowels were packed into the direct shear apparatus. A 300-lb normal load was applied to the dowels, and six loose dowels (those not taking any load) were removed from the apparatus. The load-bearing dowels can be seen in Figure 56; four arches formed in the dowel arrangement.

Figure 55. Arrangement of 67 seven-millimeter diameter dowels before applying 300-lb normal load.

Figure 56. Resulting force chains formed with a 300-lb normal load applied to the seven-millimeter dowels (six dowels were removed).

These 67 dowels were all of the same dimensions – essentially circular, 7 millimeters in diameter. The fractal fragmentation dimension, D_F, of this matrix of virtually identical units is indeterminate. No power law distribution can be discerned from this collection of identical units.

The second test was carried out by packing 64 seven-millimeter dowels and one nine-millimeter dowel into the direct shear apparatus (shown in Figure 57). Upon applying the 300-lb normal load, three arches developed and the non-load-bearing dowels were removed as shown in Figure 58. Comparing the resulting arches in this test to those formed in the uniform seven-millimeter test, it can be seen that fewer (and smaller) arches formed when the size of just one dowel was varied. With the size of one dowel varied, only three of the dowels were not engaged by the force chain, as opposed to six dowels in previous test of all seven-millimeter diameter dowels.

Figure 57. Arrangement of 64 seven-millimeter dowels and one nine-millimeter dowel before applying 300-lb normal load.

Figure 58. Resulting force chains formed with a 300-lb normal load applied to the seven-millimeter dowel matrix containing a single nine-millimeter dowel (three dowels were removed).

The fractal fragmentation dimension of the dowel matrix was changed by inserting just one dowel of a different size. It would not be practical to apply a power-law relationship to this particular distribution, but logically, by increasing the size of one of the dowels, the size-distribution of the dowels changes. Comparing the data between the first test of only identical dowels and the second test employing the same dowels with one larger dowel included in the mix, it appears that a change in the fractal fragmentation dimension of the matrix coincides with a decrease in the formation of arches in the matrix.

The third test used a matrix of 60 seven-millimeter diameter dowels with 3 nine-millimeter diameter dowels placed within the matrix (see Figure 58). Upon applying a 300-lb normal load to the dowels, only two arches formed, as shown in Figure 60. Once again, by varying the sizes of the dowels, fewer arches formed. Only three dowels were not engaged by the force chains. Although the number of loose dowels did not vary from the previous test, the number of arches formed did decrease. This indicates that more of the dowels are engaged in actively transmitting the load to the dowels surrounding them than in the previous two tests.

Similar to adding one larger dowel, adding three larger dowels to the matrix also changes the fractal fragmentation dimension of the matrix. Changing the size distribution of the dowels to be less uniform and more “well-graded” again corresponds to a decrease in the number of arches formed upon application of the 300-pound load.

Figure 59. Arrangement of 60 seven-millimeter dowels and 3 nine-millimeter dowel before applying 300-lb normal load.

Figure 60. Resulting force chains formed with a 300-lb normal load applied to the seven-millimeter dowel matrix containing 3 nine-millimeter dowels (three dowels were removed).

The results of these tests using circular dowels confirm the hypothesis that the more well-graded the distribution of dowels, the fewer arches are formed. The following tests will expand this experiment to dowels of irregular shapes, a more realistic comparison to the Machu Picchu walls.

The fourth test (Test A) used a mixture of 164 five-millimeter dowels that had been chiseled to be asymmetrical and more closely resemble the seemingly random shapes of the stones making up the walls at Machu Picchu. These dowels were packed into the direct shear apparatus (Figure 61) in the same manner as the previous tests. A normal load of 400 lbs was applied to the dowels, however, no arching developed, as shown in Figure 63. Upon reducing the normal load applied to the dowels to 300 lbs, arches developed within the matrix of dowels, as shown in Figure 64.

Figure 61. Test A –Arrangement of 164 five-millimeter irregular dowels before applying 400-lb normal load.

The dowels did not form arches when a 400-lb load was applied to them because each dowel was engaged in transmitting a portion of the load. The larger load *P* applied to the dowels generated more stress, σ, is applied as demonstrated in the following equation where A is the area over which the force is applied:

$$\sigma = \frac{P}{A} \qquad \text{(Equation 5.1)}$$

If the dowels are in a square matrix with side length *H*, as the force is applied to the matrix, it compresses an amount ΔH, as shown in Figure 61.

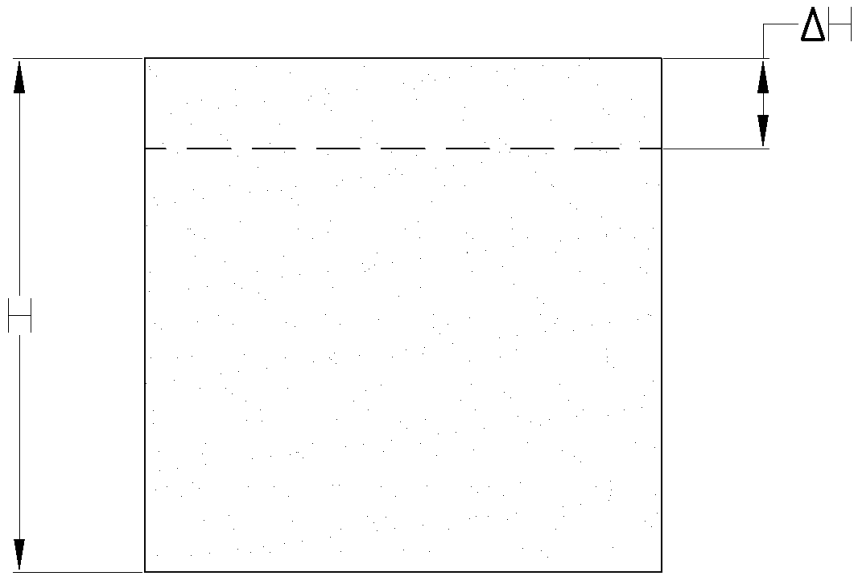

Figure 62. The dowel matrix compresses an amount ΔH when load is applied to it.

This compression causes strain in the dowels, expressed mathematically as

$$\varepsilon = \frac{\Delta H}{H} \qquad \text{(Equation 5.2)}$$

Stress and strain are related proportionally by Young's Modulus, *E*.

$$\sigma = E\varepsilon \qquad \text{(Equation 5.3)}$$

So, the greater the load/stress applied to the dowels, the greater the strain developed by the matrix. The greater strain indicates that a greater compression has occurred within the dowels. One could imagine that this compression causes the dowels to deform such that greater contact occurs between individual dowels, increasing the frictional resistance between individual dowels and engaging all of the dowels in one large force chain, transmitting the load through each dowel. The stones in the Machu Picchu walls are governed by this same law of mechanics, however, Young's Modulus for granite, estimated to be between 10.6×10^6 and 12.5×10^6 psi (Lambe and Whitman, 1969), is far greater than that for wood, estimated to be about 8×10^5 (Mamlouk and Zaniewski, 1999), thus the compression experienced by stones under the same conditions would be much less than that experienced by wood. This compression effect leads to more contact between the individual units, strengthening the wall and helping it to act as one monolithic unit rather than many small units.

Figure 63. Test A – Arrangement of 164 five-millimeter diameter irregular dowels after applying a 400-lb normal load, before reducing the load to 300 lbs. Note that no arches developed when 400 lbs was applied.

Figure 64. Test A – Force chains developed after applying 300-lb normal load to the irregular five-millimeter diameter dowels.

Figure 65 and Figure 66 show the fractal roughness and fragmentation plots, respectively. The fractal fragmentation is multi-fractal, similar to the actual walls at Machu Picchu. The fractal dimensions are summarized in Table 6.

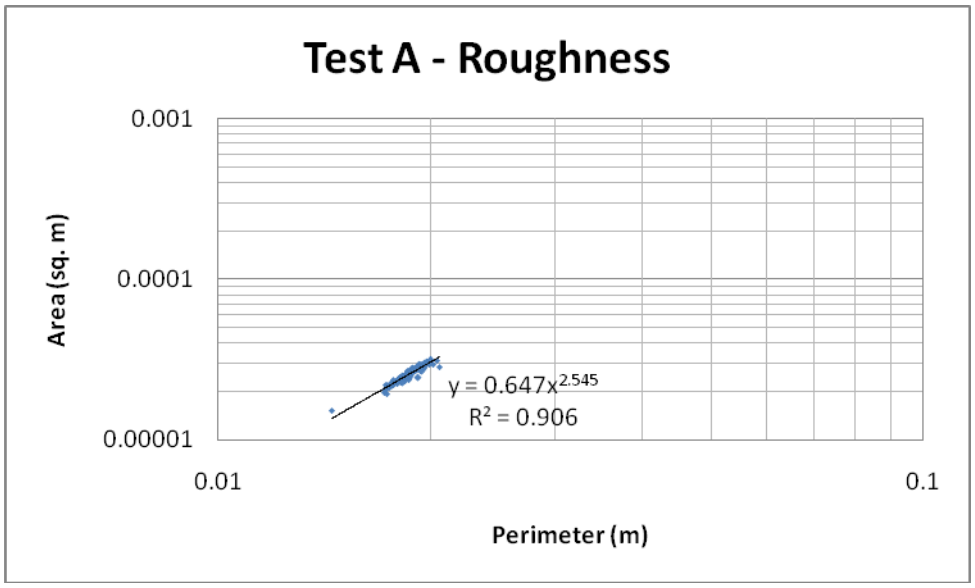

Figure 65. Test A – *P* vs. *A*

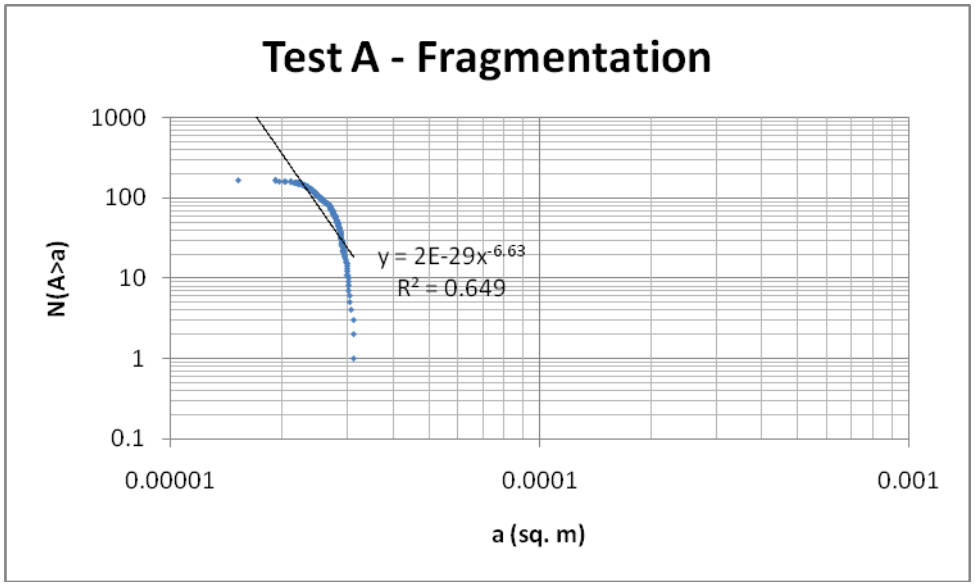

Figure 66. Test A - *a* vs. *N(A>a)*

To decrease the fractal fragmentation dimension of the dowels and create a more well-graded distribution, a single nine-millimeter dowel was placed into the five-millimeter dowel matrix for Test B, shown in Figure 67. With a 300-lb normal load applied, one arch developed as evidenced by Figure 68.

Figure 69 and Figure 70 show the plots used to determine the fractal roughness and fragmentation dimensions of the dowel distribution in Test B, summarized in Table 4 and based on a digitized image.

Figure 67. Test B – Arrangement of 159 five-millimeter irregular dowels with a single round nine-millimeter dowel before applying 300-lb normal load.

Figure 68. Test B – After applying the 300-lb normal load to the dowel matrix, no force chains developed.

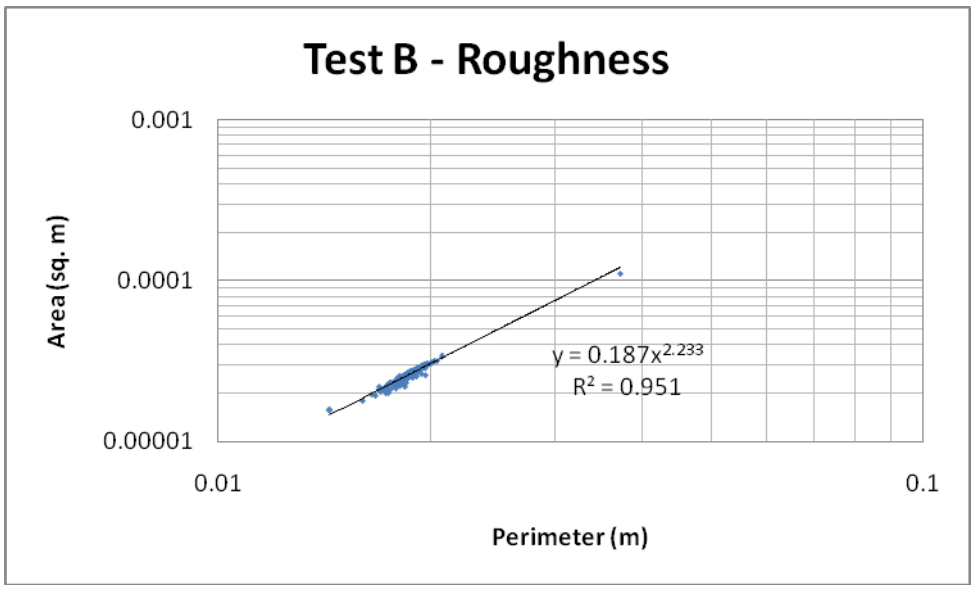

Figure 69. Test B – *P* vs. *A*

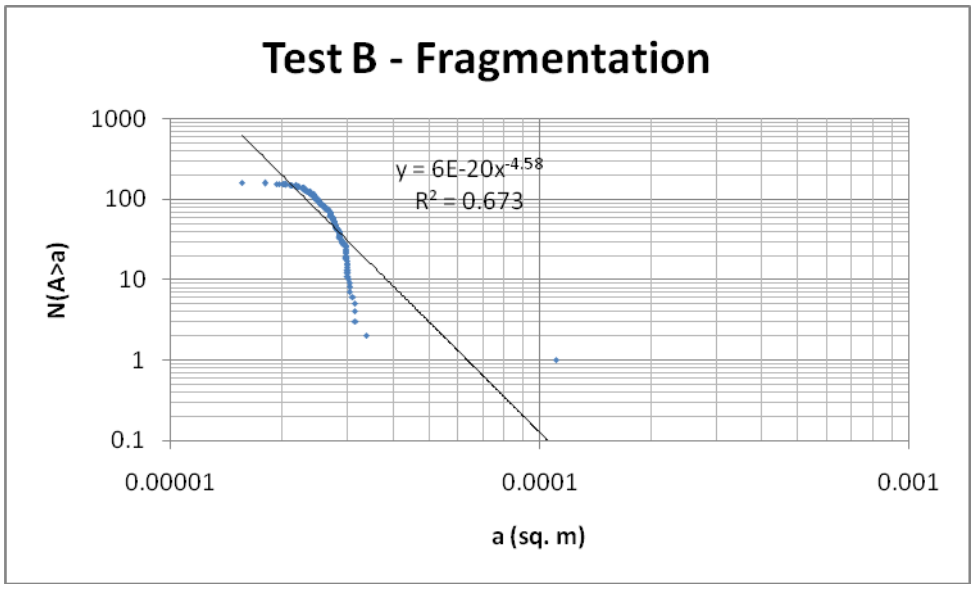

Figure 70. Test B - *a* vs. *N(A>a)*

For Test C, an additional 2 nine-millimeter dowels were added to the matrix (shown in Figure 71) to further increase the fragmentation of the matrix. As shown in Figure 72, no force chains developed.

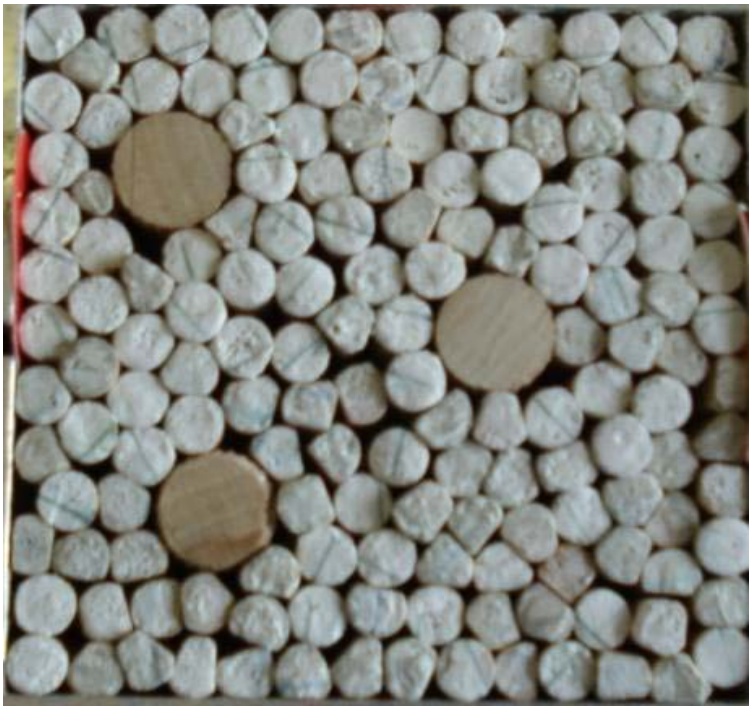

Figure 71. Test C – Arrangement of 159 irregular five-millimeter dowels with 3 nine-millimeter dowels before applying a 300-lb normal load.

Figure 72. Test C – Arrangement of mixed shape dowels after applying 300-lb normal load. No force chains developed.

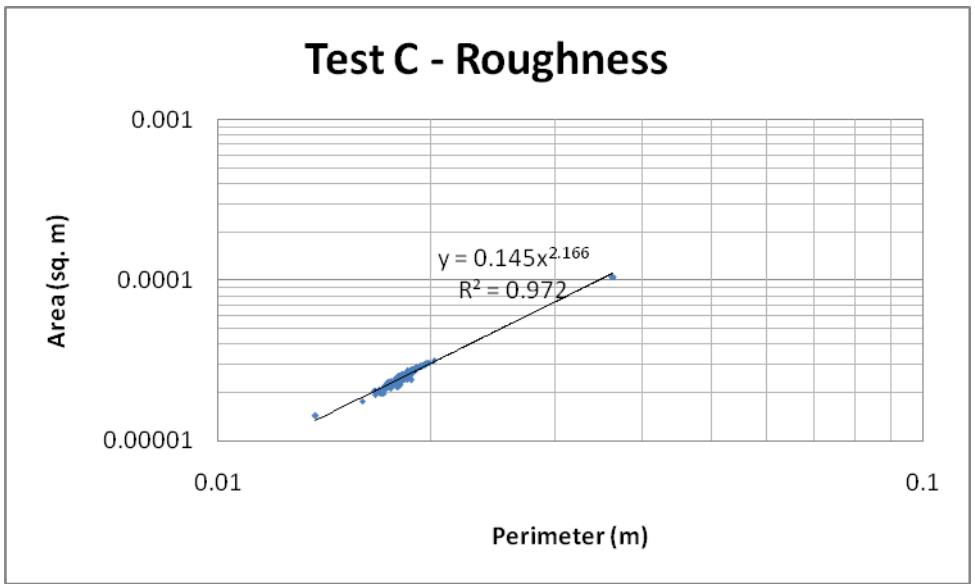

Figure 73. Test C – *P* vs. *A*

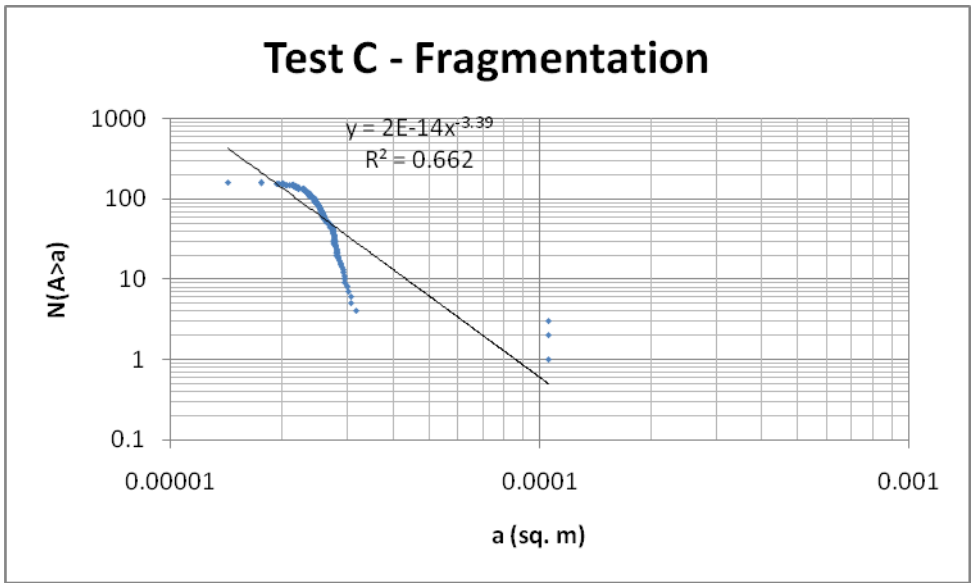

Figure 74. Test C - *a* vs. *N(A>a)*

The plots used to determine the fractal roughness and fragmentation dimensions are shown above and summarized in Table 6. The average fractal dimension once again decreased,

indicated that this distribution of dowels is even more controlled by the larger particles than those in Tests A and B.

To even further increase the fractal fragmentation of the dowel size distribution, 3 nine-millimeter and 5 seven-millimeter dowels were placed in a matrix of 153 five-millimeter irregularly-shaped dowels for Test D, as demonstrated in Figure 75. As shown in Figure 76, none of the dowels were loose and no arches formed upon applying the normal load. This arrangement also engaged each individual dowel in transmitting the forces applied to the matrix. The fractal fragmentation dimension shows that the distribution of dowels is once again even more controlled by these larger elements than in the previous tests.

Figure 75. Arrangement of 153 irregular five-millimeter dowels with 3 nine-millimeter dowels and 5 seven-millimeter dowels before applying a 300-lb normal load.

Figure 76. Arrangement of dowels after applying 300-lb normal load – no force chains developed.

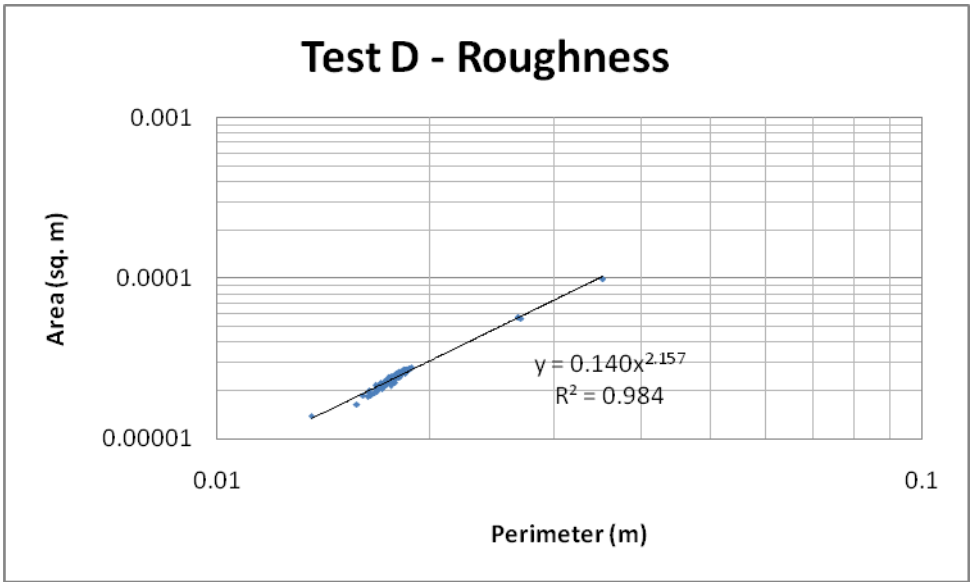

Figure 77. Test D – *P* vs. *A*

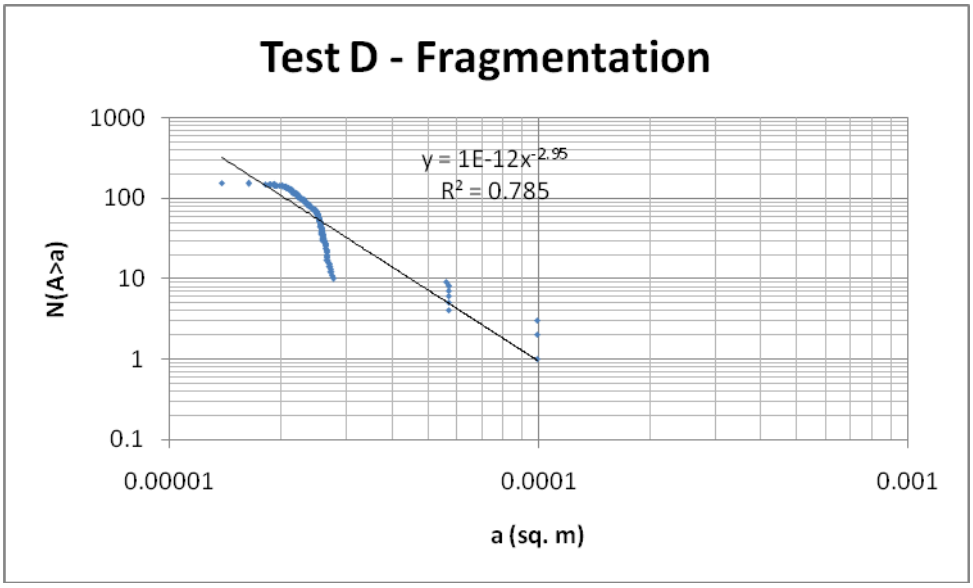

Figure 78. Test C - *a* vs. *N(A>a)*

Table 6 indicates that with each successive test, the fractal roughness dimension, D_R, increased (indicating a greater variety of perimeter shapes) and the average fragmentation dimension, D_F, decreased as the slope of the line was influced by the larger dowels (indicating a more well-graded mixture of dowel sizes). The fragmentation dimension of the dowel tests is approaching the near-unity values of D_F calculated for the retaining walls. This suggests that the Incan walls are actually made up of a more well-graded distribution than even the dowels in Test D, correlating with the lack of pop-out and toppling failures in the Incan walls.

The behavior summarized by these tests is significant for the Incan walls because their composition is characterized by a wide range of stone sizes and roughness, similar to that of Test D. While the identical dowels allowed more arches to develop, the varied dowels formed fewer arches, because the varied sizes permitted more contact between the dowels and thus forces are distributed in a more even fashion throughout the stones. The force of soil pushing against the wall was simulated by pulling the dowels out with tweezers. If the retaining walls at Machu

Picchu weren't engaging most of the stones making them up, the soil pushing against the wall would force out the stones not engaged in the force chains, forming gaping arches where the soil behind the walls could easily fall out from behind the wall. The lateral loads imposed by the remaining soil behind the wall would be transferred to the remaining stones via the arching effects of soil, causing widespread failures in the wall.

Table 6. Fractal Dimensions for laboratory Tests A, B, C, and D.

	D_R	R^2	D_F	R^2	Arches Formed
Test A	0.786	0.906	13.3	0.649	8
Test B	0.896	0.951	9.16	0.673	1
Test C	0.923	0.972	6.78	0.662	0
Test D	0.927	0.984	5.90	0.785	0

The Inca engineers may have known this – building walls at Machu Picchu generally exhibit much more uniform construction (as demonstrated in Section 4.2), while the retaining walls are made up of varying sizes of stones. Perhaps this was an aesthetic choice; most likely the walls are made up of varying sizes of stones because these retaining walls are of less "importance". Most of the complex, more aesthetically-pleasing stone work was likely reserved for more important areas such as the royal residence or sacred sites.

5.4 STABILITY ANALYSIS REVISITED

As demonstrated, Machu Picchu's retaining walls have a fractal size distribution as well as a fractal roughness. As shown via the laboratory simulation with the direct shear apparatus, the size distribution of the individual units is directly related to the amount of contact between the units. When a set of uniform-sized dowels were tested, arches developed in the matrix, proving that these dowels were not effectively transmitting loads through their contacts to their full potential.

The stability analysis conducted in Section 3.0 assumed that friction was developed on the entire surface area of the 1-ft by 2.5-ft block. However, the stability analysis also assumed that the blocks were of a uniform size distribution. If the uniform-sized blocks in this analysis behaved like the dowels studied in the laboratory simulation, these stones would not be fully engaged in transmitting the load to one another and the contact between blocks would be reduced. In the case of a popout failure, assuming that the bottom block of the wall was not engaged with the stones above it, the normal force applied at the base of that block is only the weight of the block itself, rather than the weight of the entire wall above it. It is also only developing friction along its bottom, not the top. If this were the case, the popout factor of safety would be reduced from 12.0 (as demonstrated in the initial stability analysis) to just 0.920, which is not only up to our modern standards but is below unity, indicative of a failure.

This supports the hypothesis that the retaining walls at Machu Picchu garner at least some of their inherent stability from the effects of fractals; the more effective packing of stones of multiple sizes increases the effective transmission of loads through every particle in the wall, engaging it in one monolithic structure.

6.0 CONCLUSION

The retaining walls at Machu Picchu are well-built and have endured with essentially no maintenance since the city was abandoned centuries ago. The modular gravity granite block walls were built on appropriately prepared foundations and exhibit adequate factors of safety against sliding and overturning, generally comparable to those required by today's engineers.

The walls have a fractal dimension in terms of roughness. The analysis carried out indicates that the fractal roughness dimension varies from 0.94 to 1.16. The structural roughness of the walls facilitates more contact between the individual wall elements, adding to the stability of the wall. The distribution of elements in the wall is also fractal. This analysis shows that they are actually multi-fractal over several ranges. This variety of sizes also encourages more contact between the individual units making up the walls.

Via laboratory analogy with wooden dowels compressed in a direct shear apparatus, it is confirmed that the fractal size distribution of the units making up the Machu Picchu walls contributes to their stability; the more "well-graded" the matrix, the more contact forms between the particles, thus each of the units is engaged in carrying the load applied to it.

Had the walls at Machu Picchu been constructed of identically-sized stones, fewer contacts would exist between each of the stones in the walls. Fewer contacts between adjacent stones would limit the transmission of loads between neighboring stones, effectively decreasing the stability of the walls. The fractal distribution of units in the wall maximizes the packing of

stones within the wall while still allowing gaps between the stones to dissipate hydrostatic pressure behind the wall.

In the future, this study may be improved by using other techniques (such as a different digitizing system) to examine the fractal aspects of the walls. A more accurate stability analysis could be conducted given more specific information about the conditions encountered in Machu Picchu, should future excavations or test borings be permitted at the site to glean the appropriate engineering properties of the soil. Given well-publicized recent tectonic activity in western South America, a more detailed seismic study could be conducted to gather information about the Incan engineers' knowledge of seismic design.

Today's modular retaining walls may be improved by considering a fractal distribution of units throughout the wall. Precast concrete units of various sizes with substantial roughness could easily be mass-produced and sold as a package for retaining wall construction. Rather than manufacturing 900 units of "Size X," manufacturers could produce 300 units of "Size X," 300 units of "Size Y," and 300 units of "Size Z." Combining the concept of fractals with modern modular wall design could lead to longer-lasting, more stable retaining walls.

Perhaps the Incan engineers, through their experiences in other areas of their empire, observed these principals at work (through trial and error) and intentionally constructed the walls with a fractal distribution and adequate factors of safety. Perhaps it was an aesthetic choice. Perhaps the choice was driven by economics. If the Incan engineers thought the way modern engineers think, it was a combination of all of these factors. Regardless of the motivation, the Incan engineers knew how to construct lasting infrastructure. The Incan infrastructure withstood centuries of neglect and remains intact; much of our modern infrastructure receives some

maintenance (though frequently not nearly as much as it should) and still fails much sooner than that of the Incan empire.

The concept of fractals can be applied to the retaining walls of Machu Picchu and several aspects of geotechnical engineering, including crushing of granular materials and grain-size distribution analysis. Perhaps fractal theory will make its way into other civil engineering disciplines. Someday engineers may find ways to employ them in the design and analysis of bridges, structures, pavements, or water systems.

APPENDIX A

TABULATION OF WALL UNIT AREAS AND PERIMETERS

A.1 WALL 1

Stone	Area (m^2)	Perim. (m)	N(A>a)
147	0.667	3.65	0
14	0.325	2.49	1
33	0.214	1.86	2
73	0.212	1.92	3
120	0.171	1.81	4
137	0.161	1.92	5
203	0.125	1.51	6
172	0.104	1.29	7
153	0.0857	1.24	8
54	0.0779	1.05	9
50	0.0766	1.12	10
88	0.0766	1.04	11
105	0.0751	1.12	12
138	0.0701	1.16	13
215	0.0699	1.05	14
8	0.0697	1.02	15
30	0.0661	1.07	16
85	0.0658	0.972	17
200	0.0655	1.02	18
205	0.0638	1.09	19
194	0.0631	0.969	20
66	0.0619	0.994	21
36	0.0606	1.04	22

Stone	Area (m^2)	Perim. (m)	N(A>a)
214	0.0587	0.988	23
249	0.0575	1.02	24
181	0.0560	0.945	25
6	0.0552	0.949	26
99	0.0534	0.937	27
252	0.0530	1.103	28
76	0.0518	0.940	29
133	0.0512	0.850	30
93	0.0512	0.918	31
34	0.0508	0.894	32
11	0.0497	0.856	33
139	0.0490	0.856	34
127	0.0485	0.883	35
5	0.0472	0.829	36
173	0.0471	0.899	37
213	0.0458	0.814	38
16	0.0454	0.845	39
45	0.0450	0.891	40
107	0.0450	0.866	41
245	0.0447	0.848	42
224	0.0445	0.849	43
117	0.0433	0.813	44
37	0.0431	0.810	45

Stone	Area (m^2)	Perim. (m)	N(A>a)
81	0.0426	0.821	46
53	0.0425	0.800	47
57	0.0425	1.04	48
175	0.0419	0.845	49
38	0.0417	0.827	50
240	0.0414	0.837	51
196	0.0411	0.811	52
142	0.0408	0.794	53
199	0.0408	0.863	54
146	0.0406	0.774	55
174	0.0404	0.794	56
218	0.0403	0.759	57
145	0.0400	0.777	58
230	0.0397	0.842	59
2	0.0396	0.961	60
124	0.0395	0.791	61
129	0.0395	0.757	62
166	0.0388	0.787	63
162	0.0388	0.824	64
242	0.0385	0.907	65
77	0.0378	0.877	66
96	0.0378	0.796	67
141	0.0371	0.750	68
189	0.0370	0.776	69
70	0.0369	0.796	70
177	0.0368	0.785	71
110	0.0367	0.958	72
225	0.0366	0.766	73
18	0.0359	0.822	74
25	0.0358	0.753	75
187	0.0356	0.764	76
206	0.0353	0.752	77
84	0.0348	0.806	78
78	0.0345	0.727	79
22	0.0333	0.787	80
202	0.0327	0.820	81
250	0.0325	0.730	82
82	0.0325	0.712	83
134	0.0324	0.821	84
234	0.0323	0.673	85

Stone	Area (m^2)	Perim. (m)	N(A>a)
115	0.0323	0.742	86
149	0.0323	0.788	87
170	0.0322	0.755	88
157	0.0320	0.767	89
219	0.0313	0.746	90
158	0.0312	0.745	91
15	0.0311	0.766	92
111	0.0303	0.790	93
185	0.0301	0.731	94
223	0.0295	0.689	95
238	0.0288	0.662	96
243	0.0281	0.725	97
109	0.0280	0.730	98
126	0.0280	0.673	99
48	0.0278	0.820	100
154	0.0274	0.743	101
220	0.0272	0.699	102
204	0.0264	0.614	103
246	0.0261	0.755	104
1	0.0261	0.599	105
104	0.0260	0.668	106
144	0.0258	0.637	107
29	0.0248	0.635	108
4	0.0246	0.677	109
21	0.0244	0.685	110
171	0.0241	0.644	111
40	0.0240	0.660	112
113	0.0237	0.610	113
31	0.0228	0.581	114
55	0.0224	0.695	115
253	0.0224	0.633	116
67	0.0218	0.552	117
39	0.0211	0.588	118
27	0.0210	0.624	119
161	0.0210	0.608	120
7	0.0209	0.545	121
184	0.0195	0.594	122
193	0.0194	0.572	123
9	0.0193	0.521	124
227	0.0187	0.520	125

Stone	Area (m^2)	Perim. (m)	N(A>a)
216	0.0185	0.540	126
23	0.0182	0.520	127
119	0.0172	0.515	128
12	0.0156	0.690	129
192	0.0145	0.513	130
176	0.0139	0.533	131
163	0.0129	0.460	132
217	0.0128	0.487	133
60	0.0124	0.415	134
244	0.0121	0.432	135
237	0.0120	0.459	136
239	0.0115	0.607	137
221	0.0110	0.430	138
241	0.0108	0.494	139
148	0.0107	0.398	140
156	0.0104	0.566	141
112	0.0100	0.396	142
251	0.00954	0.471	143
165	0.00917	0.395	144
198	0.00890	0.365	145
235	0.00864	0.528	146
19	0.00861	0.386	147
210	0.00832	0.400	148
100	0.00816	0.388	149
17	0.00782	0.425	150
121	0.00746	0.340	151
83	0.00740	0.398	152
151	0.00738	0.354	153
75	0.00736	0.327	154
49	0.00732	0.463	155
197	0.00727	0.401	156
116	0.00706	0.335	157
236	0.00700	0.329	158
123	0.00698	0.367	159
62	0.00666	0.327	160
122	0.00659	0.386	161
72	0.00637	0.335	162
180	0.00611	0.357	163
90	0.00581	0.388	164
51	0.00580	0.381	165

Stone	Area (m^2)	Perim. (m)	N(A>a)
10	0.00553	0.364	166
140	0.00553	0.299	167
28	0.00540	0.365	168
150	0.00521	0.408	169
229	0.00512	0.291	170
231	0.00511	0.308	171
211	0.00507	0.310	172
71	0.00506	0.267	173
35	0.00504	0.331	174
68	0.00491	0.293	175
86	0.00490	0.291	176
95	0.00460	0.282	177
20	0.00458	0.284	178
97	0.00455	0.277	179
108	0.00434	0.386	180
59	0.00433	0.254	181
114	0.00428	0.273	182
136	0.00407	0.259	183
69	0.00387	0.247	184
87	0.00385	0.251	185
152	0.00373	0.295	186
106	0.00372	0.267	187
254	0.00354	0.218	188
3	0.00351	0.304	189
42	0.00340	0.242	190
228	0.00332	0.243	191
201	0.00321	0.250	192
74	0.00312	0.239	193
232	0.00309	0.230	194
98	0.00301	0.214	195
63	0.00300	0.259	196
135	0.00296	0.248	197
186	0.00283	0.212	198
143	0.00281	0.211	199
159	0.00271	0.217	200
233	0.00269	0.222	201
195	0.00268	0.206	202
190	0.00264	0.201	203
13	0.00260	0.205	204
94	0.00256	0.203	205

Stone	Area (m^2)	Perim. (m)	N(A>a)
160	0.00250	0.207	206
58	0.00245	0.290	207
226	0.00237	0.200	208
56	0.00233	0.226	209
248	0.00227	0.220	210
179	0.00211	0.201	211
155	0.00190	0.199	212
183	0.00187	0.185	213
125	0.00182	0.171	214
191	0.00179	0.157	215
118	0.00177	0.163	216
61	0.00171	0.210	217
46	0.00167	0.167	218
222	0.00158	0.168	219

Stone	Area (m^2)	Perim. (m)	N(A>a)
80	0.00151	0.161	220
79	0.00149	0.151	221
128	0.00141	0.161	222
247	0.00139	0.198	223
26	0.00133	0.161	224
91	0.00125	0.186	225
188	0.00119	0.165	226
178	0.000901	0.122	227
212	0.000855	0.178	228
32	0.000845	0.111	229
24	0.000827	0.119	230
164	0.000604	0.112	231
92	0.000381	0.0998	232
89	0.000316	0.0736	233

A.2 WALL 2

Stone	Area (m^2)	Perim. (m)	N(A>a)
74	0.620	3.06	0
13	0.608	3.11	1
41	0.350	2.29	2
88	0.227	1.92	3
17	0.135	1.46	4
62	0.111	1.32	5
18	0.111	1.47	6
101	0.0893	1.45	7
14	0.0892	1.28	8
9	0.0764	1.16	9
28	0.0689	1.04	10
81	0.0623	1.09	11
80	0.0594	0.967	12
8	0.0554	1.09	13
63	0.0530	0.898	14
44	0.0482	0.839	15

Stone	Area (m^2)	Perim. (m)	N(A>a)
7	0.0466	0.897	16
99	0.0402	0.803	17
12	0.0397	0.792	18
96	0.0370	0.776	19
32	0.0366	0.821	20
47	0.0356	0.828	21
69	0.0335	0.795	22
53	0.0299	0.669	23
39	0.0254	0.682	24
72	0.0235	0.645	25
26	0.0230	0.596	26
75	0.0226	0.674	27
30	0.0193	0.526	28
57	0.0175	0.599	29
6	0.0161	0.517	30
61	0.0150	0.574	31

Stone	Area (m^2)	Perim. (m)	N(A>a)
36	0.0138	0.502	32
4	0.0133	0.430	33
48	0.0121	0.505	34
85	0.0114	0.554	35
56	0.0114	0.512	36
35	0.0102	0.451	37
83	0.0100	0.442	38
93	0.00952	0.409	39
38	0.00896	0.456	40
5	0.00847	0.386	41
25	0.00807	0.388	42
87	0.00707	0.412	43
15	0.00699	0.352	44
76	0.00699	0.339	45
100	0.00697	0.343	46
46	0.00661	0.334	47
43	0.00638	0.332	48
34	0.00624	0.332	49
50	0.00544	0.353	50
45	0.00519	0.391	51
55	0.00475	0.285	52
40	0.00465	0.389	53
33	0.00449	0.275	54
94	0.00445	0.312	55
11	0.00439	0.371	56
70	0.00416	0.313	57

Stone	Area (m^2)	Perim. (m)	N(A>a)
89	0.00407	0.304	58
102	0.00387	0.262	59
90	0.00386	0.232	60
19	0.00372	0.243	61
103	0.00353	0.272	62
42	0.00327	0.268	63
27	0.00317	0.221	64
79	0.00308	0.226	65
3	0.00306	0.238	66
16	0.00306	0.233	67
29	0.00282	0.220	68
49	0.00264	0.240	69
20	0.00221	0.229	70
84	0.00154	0.200	71
24	0.00120	0.136	72
54	0.00108	0.139	73
86	0.000715	0.103	74
60	0.000492	0.0937	75
37	0.000465	0.0929	76
78	0.000455	0.0873	77
73	0.000418	0.118	78
82	0.000418	0.0896	79
77	0.000269	0.0968	80
52	0.000223	0.0645	81
106	0.000204	0.0703	82
51	0.000195	0.0638	83

A.3 WALL 3

Stone	Area (m^2)	Perim. (m)	N(A>a)
53	0.404	2.83	0
12	0.127	1.44	1
25	0.0963	1.22	2
15	0.0841	1.25	3
72	0.0813	1.12	4
111	0.0812	1.11	5
50	0.0807	1.08	6
80	0.0715	1.07	7
74	0.0701	1.06	8
43	0.0670	1.05	9
51	0.0662	1.06	10
57	0.0644	1.05	11
91	0.0639	0.988	12
70	0.0634	1.11	13
10	0.0615	1.17	14
2	0.0611	1.22	15
131	0.0605	0.989	16
48	0.0594	1.01	17
81	0.0498	0.892	18
17	0.0493	0.846	19
37	0.0493	0.900	20
104	0.0470	0.851	21
47	0.0436	0.831	22
101	0.0426	0.941	23
119	0.0412	0.813	24
97	0.0408	0.795	25
79	0.0391	0.822	26
78	0.0385	0.847	27
125	0.0367	0.737	28
9	0.0360	0.848	29
82	0.0359	0.799	30
29	0.0348	0.776	31
130	0.0348	0.723	32

Stone	Area (m^2)	Perim. (m)	N(A>a)
42	0.0341	0.789	33
95	0.0337	0.772	34
21	0.0332	0.748	35
114	0.0328	0.823	36
77	0.0327	0.801	37
88	0.0318	0.703	38
86	0.0281	0.635	39
30	0.0267	0.666	40
112	0.0267	0.677	41
75	0.0258	0.693	42
135	0.0245	0.606	43
85	0.0242	0.665	44
55	0.0237	0.673	45
106	0.0231	0.644	46
120	0.0230	0.613	47
113	0.0229	0.651	48
26	0.0225	0.550	49
6	0.0213	0.707	50
11	0.0209	0.573	51
92	0.0201	0.634	52
93	0.0197	0.587	53
121	0.0178	0.516	54
8	0.0172	0.691	55
23	0.0165	0.578	56
137	0.0163	0.540	57
5	0.0162	0.630	58
4	0.0152	0.550	59
7	0.0149	0.536	60
49	0.0147	0.473	61
54	0.0127	0.598	62
59	0.0106	0.419	63
44	0.0101	0.417	64
96	0.00988	0.429	65

Stone	Area (m^2)	Perim. (m)	N(A>a)
73	0.00983	0.399	66
99	0.00949	0.373	67
60	0.00929	0.379	68
123	0.00901	0.454	69
33	0.00813	0.366	70
84	0.00793	0.456	71
64	0.00775	0.338	72
31	0.00765	0.351	73
89	0.00715	0.331	74
38	0.00710	0.373	75
63	0.00703	0.421	76
100	0.00675	0.360	77
128	0.00659	0.459	78
56	0.00653	0.317	79
18	0.00623	0.319	80
46	0.00598	0.353	81
52	0.00441	0.274	82
27	0.00414	0.273	83
127	0.00355	0.323	84
102	0.00341	0.259	85
94	0.00331	0.296	86
105	0.00320	0.245	87
71	0.00308	0.256	88
122	0.00283	0.223	89

Stone	Area (m^2)	Perim. (m)	N(A>a)
98	0.00280	0.223	90
136	0.00280	0.208	91
117	0.00260	0.223	92
115	0.00258	0.224	93
126	0.00202	0.214	94
109	0.00185	0.231	95
20	0.00178	0.177	96
118	0.00171	0.174	97
3	0.00168	0.165	98
87	0.00168	0.184	99
39	0.00164	0.166	100
90	0.00163	0.199	101
124	0.00139	0.183	102
110	0.00116	0.197	103
40	0.00106	0.130	104
129	0.000864	0.112	105
116	0.000836	0.153	106
76	0.000790	0.165	107
108	0.000780	0.112	108
103	0.000715	0.160	109
83	0.000576	0.129	110
132	0.000576	0.0925	111
107	0.000511	0.0915	112

A.4 WALL 4

Stone	Area (m^2)	Perim. (m)	N(A>a)
61	0.345	2.31	0
55	0.284	2.22	1
126	0.183	1.89	2
33	0.176	1.76	3
165	0.147	1.78	4
158	0.0789	1.08	5
64	0.0762	1.14	6
215	0.0760	1.13	7
114	0.0661	1.16	8
11	0.0640	1.09	9
72	0.0629	0.312	10
106	0.0619	1.02	11
22	0.0587	1.03	12
274	0.0579	1.09	13
116	0.0549	1.07	14
289	0.0546	0.913	15
295	0.0539	0.949	16
121	0.0519	0.889	17
110	0.0508	0.899	18
237	0.0506	0.942	19
197	0.0504	0.914	20
137	0.0473	0.878	21
177	0.0464	0.897	22
171	0.0441	0.857	23
224	0.0436	0.900	24
91	0.0417	0.797	25
70	0.0416	0.861	26
82	0.0399	0.808	27
218	0.0397	0.861	28
283	0.0394	0.790	29
140	0.0388	0.820	30
77	0.0386	0.861	31
297	0.0382	0.894	32

Stone	Area (m^2)	Perim. (m)	N(A>a)
270	0.0381	0.779	33
100	0.0364	0.766	34
258	0.0352	0.707	35
183	0.0352	0.772	36
123	0.0346	0.794	37
34	0.0346	0.707	38
286	0.0345	0.748	39
58	0.0337	0.756	40
73	0.0332	0.763	41
266	0.0300	0.682	42
238	0.0298	0.721	43
190	0.0289	0.700	44
138	0.0286	0.819	45
208	0.0270	0.617	46
66	0.0252	0.686	47
299	0.0242	0.648	48
221	0.0240	0.611	49
281	0.0227	0.642	50
10	0.0214	0.594	51
230	0.0213	0.610	52
234	0.0212	0.631	53
5	0.0206	0.715	54
153	0.0205	0.628	55
235	0.0203	0.534	56
213	0.0195	0.598	57
31	0.0192	0.568	58
273	0.0191	0.533	59
252	0.0191	0.564	60
19	0.0190	0.549	61
189	0.0174	0.502	62
86	0.0165	0.546	63
20	0.0164	0.486	64
29	0.0161	0.526	65

Stone	Area (m^2)	Perim. (m)	N(A>a)
79	0.0153	0.641	66
63	0.0152	0.592	67
260	0.0145	0.461	68
161	0.0144	0.491	69
21	0.0141	0.477	70
119	0.0141	0.519	71
199	0.0139	0.525	72
78	0.0138	0.453	73
6	0.0135	0.490	74
50	0.0128	0.434	75
173	0.0121	0.436	76
223	0.0119	0.445	77
298	0.0119	0.464	78
49	0.0118	0.453	79
12	0.0112	0.424	80
81	0.0112	0.424	81
259	0.0110	0.400	82
156	0.0109	0.422	83
84	0.0107	0.432	84
83	0.0104	0.483	85
180	0.0101	0.406	86
112	0.0101	0.393	87
194	0.00983	0.418	88
145	0.00960	0.381	89
46	0.00943	0.386	90
210	0.00943	0.372	91
225	0.00937	0.368	92
87	0.00886	0.389	93
206	0.00874	0.038	94
59	0.00869	0.373	95
75	0.00867	0.350	96
71	0.00854	0.418	97
157	0.00849	0.422	98
164	0.00844	0.391	99
51	0.00838	0.372	100
229	0.00836	0.363	101
214	0.00820	0.373	102
56	0.00818	0.377	103
76	0.00817	0.381	104
179	0.00799	0.400	105

Stone	Area (m^2)	Perim. (m)	N(A>a)
134	0.00781	0.373	106
62	0.00780	0.404	107
139	0.00735	0.381	108
129	0.00717	0.358	109
103	0.00709	0.395	110
261	0.00709	0.352	111
52	0.00687	0.343	112
150	0.00653	0.305	113
135	0.00652	0.343	114
166	0.00641	0.401	115
107	0.00637	0.321	116
54	0.00631	0.331	117
267	0.00630	0.347	118
132	0.00623	0.302	119
105	0.00609	0.347	120
255	0.00604	0.310	121
216	0.00565	0.387	122
226	0.00561	0.313	123
239	0.00558	0.286	124
89	0.00556	0.281	125
95	0.00555	0.328	126
104	0.00552	0.302	127
144	0.00540	0.300	128
69	0.00534	0.318	129
174	0.00529	0.299	130
172	0.00516	0.323	131
67	0.00506	0.267	132
219	0.00504	0.283	133
28	0.00481	0.301	134
212	0.00472	0.275	135
133	0.00471	0.326	136
99	0.00468	0.298	137
131	0.00455	0.287	138
127	0.00443	0.353	139
290	0.00440	0.285	140
9	0.00437	0.257	141
25	0.00436	0.263	142
244	0.00434	0.251	143
186	0.00431	0.263	144
202	0.00428	0.311	145

Stone	Area (m^2)	Perim. (m)	N(A>a)
27	0.00425	0.294	146
302	0.00425	0.262	147
204	0.00419	0.275	148
109	0.00418	0.263	149
122	0.00418	0.315	150
170	0.00413	0.324	151
195	0.00410	0.250	152
15	0.00404	0.275	153
130	0.00401	0.294	154
143	0.00395	0.360	155
253	0.00389	0.282	156
65	0.00387	0.245	157
152	0.00386	0.245	158
162	0.00380	0.254	159
149	0.00373	0.251	160
92	0.00369	0.233	161
142	0.00369	0.251	162
60	0.00367	0.244	163
128	0.00358	0.260	164
30	0.00352	0.246	165
160	0.00348	0.242	166
181	0.00347	0.243	167
155	0.00345	0.242	168
111	0.00342	0.246	169
280	0.00333	0.238	170
251	0.00331	0.286	171
231	0.00330	0.242	172
285	0.00315	0.234	173
222	0.00313	0.230	174
191	0.00311	0.240	175
294	0.00308	0.314	176
233	0.00290	0.212	177
282	0.00288	0.207	178
296	0.00286	0.266	179
115	0.00278	0.231	180
178	0.00278	0.258	181
39	0.00272	0.258	182
243	0.00266	0.200	183
97	0.00260	0.229	184
188	0.00258	0.266	185

Stone	Area (m^2)	Perim. (m)	N(A>a)
175	0.00255	0.243	186
265	0.00255	0.206	187
113	0.00246	0.219	188
228	0.00242	0.210	189
48	0.00239	0.212	190
263	0.00239	0.233	191
88	0.00226	0.208	192
120	0.00226	0.228	193
304	0.00219	0.187	194
37	0.00218	0.201	195
196	0.00214	0.194	196
117	0.00211	0.208	197
287	0.00211	0.191	198
198	0.00206	0.205	199
176	0.00191	0.206	200
232	0.00187	0.177	201
169	0.00186	0.165	202
182	0.00184	0.185	203
90	0.00178	0.203	204
146	0.00173	0.217	205
168	0.00171	0.223	206
167	0.00169	0.194	207
200	0.00164	0.161	208
18	0.00162	0.183	209
271	0.00156	0.159	210
124	0.00155	0.162	211
192	0.00151	0.162	212
96	0.00148	0.209	213
118	0.00142	0.176	214
249	0.00135	0.161	215
141	0.00134	0.231	216
292	0.00132	0.166	217
74	0.00131	0.154	218
108	0.00124	0.150	219
220	0.00122	0.165	220
57	0.00119	0.149	221
264	0.00116	0.131	222
184	0.00113	0.172	223
205	0.00113	0.135	224
209	0.00113	0.143	225

Stone	Area (m^2)	Perim. (m)	N(A>a)
201	0.00111	0.135	226
217	0.00111	0.133	227
293	0.00109	0.154	228
17	0.00108	0.143	229
98	0.00108	0.141	230
7	0.000975	0.150	231
236	0.000966	0.124	232
275	0.000883	0.137	233
93	0.000845	0.129	234
227	0.000845	0.119	235
187	0.000780	0.109	236
207	0.000771	0.108	237
94	0.000753	0.111	238
136	0.000697	0.100	239
148	0.000687	0.102	240
159	0.000632	0.101	241

Stone	Area (m^2)	Perim. (m)	N(A>a)
193	0.000567	0.122	242
279	0.000539	0.110	243
203	0.000474	0.0881	244
125	0.000465	0.0874	245
163	0.000455	0.108	246
3	0.000437	0.0778	247
47	0.000437	0.112	248
68	0.000409	0.0799	249
38	0.000316	0.0988	250
262	0.000269	0.0780	251
185	0.000223	0.0650	252
102	0.000204	0.0541	253
53	0.000158	0.0598	254
278	0.000139	0.0484	255
301	9.29E-05	0.0357	256
101	4.65E-05	0.0243	257

A.5 WALL 5

Stone	Area (m^2)	Perim. (m)	N(A>a)
199	0.146	1.75	0
75	0.145	1.68	1
208	0.142	1.53	2
136	0.133	1.57	3
19	0.121	1.61	4
132	0.110	1.50	5
192	0.106	1.29	6
195	0.106	1.25	7
185	0.105	1.32	8
193	0.104	1.42	9
228	0.0999	1.40	10
32	0.0936	1.27	11
220	0.0928	1.26	12
26	0.0924	1.45	13
135	0.0917	1.24	14
97	0.0901	1.25	15

Stone	Area (m^2)	Perim. (m)	N(A>a)
78	0.0887	1.21	16
226	0.0875	1.15	17
196	0.0853	1.28	18
212	0.0847	1.37	19
215	0.0805	1.19	20
85	0.0789	1.18	21
134	0.0773	1.27	22
91	0.0770	1.11	23
96	0.0762	1.21	24
142	0.0749	1.15	25
83	0.0735	1.23	26
86	0.0735	1.12	27
227	0.0733	1.14	28
92	0.0708	1.09	29
38	0.0696	1.30	30
29	0.0691	1.27	31

Stone	Area (m^2)	Perim. (m)	N(A>a)
191	0.0687	1.02	32
205	0.0687	1.03	33
36	0.0684	1.17	34
197	0.0634	1.01	35
93	0.0623	1.08	36
131	0.0620	1.07	37
17	0.0620	1.15	38
89	0.0615	0.944	39
190	0.0613	1.00	40
143	0.0601	1.24	41
211	0.0580	1.26	42
20	0.0578	1.06	43
87	0.0572	1.19	44
16	0.0556	0.909	45
224	0.0538	0.973	46
139	0.0523	1.03	47
15	0.0497	0.876	48
80	0.0484	0.837	49
21	0.0471	0.903	50
221	0.0469	0.850	51
90	0.0456	0.829	52
33	0.0454	0.896	53
77	0.0444	0.916	54
222	0.0444	1.09	55
31	0.0430	1.04	56
214	0.0419	0.793	57
95	0.0417	0.850	58
24	0.0386	0.771	59
210	0.0359	0.915	60
138	0.0339	0.975	61
202	0.0326	0.802	62
82	0.0324	0.758	63
34	0.0302	0.675	64

Stone	Area (m^2)	Perim. (m)	N(A>a)
79	0.0296	0.676	65
217	0.0296	0.673	66
144	0.0276	0.629	67
137	0.0270	0.764	68
203	0.0248	0.792	69
94	0.0235	0.589	70
28	0.0232	0.577	71
88	0.0215	0.568	72
225	0.0208	0.554	73
209	0.0199	0.537	74
22	0.0191	0.732	75
25	0.0187	0.511	76
18	0.0170	0.596	77
23	0.0167	0.538	78
213	0.0130	0.478	79
84	0.0106	0.481	80
207	0.00937	0.383	81
218	0.00805	0.617	82
216	0.00728	0.412	83
27	0.00699	0.534	84
194	0.00685	0.336	85
198	0.00450	0.319	86
81	0.00372	0.268	87
219	0.00360	0.263	88
133	0.00352	0.277	89
140	0.00349	0.297	90
204	0.00339	0.360	91
200	0.00293	0.498	92
201	0.00261	0.271	93
206	0.00193	0.164	94
223	0.00159	0.172	95
141	0.00118	0.159	96

BIBLIOGRAPHY

ABC-CLIO. (2001). Encyclopedia of Archaeology: History and Discoveries. Retrieved April 2009, from Inca: http://www.credoreference.com/engry/8056707.

ABC-CLIO. (2001). Encyclopedia of Archaeology: History and Discoveries. Retrieved April 2009, from Machu Picchu: http://www.credoreference.com/engry/8056789.

AUTOCAD LT. Autodesk, Inc., 2007.

Boast, C.W. and Baveye, P., "Fractal Geometry, Fragmentation Processes and the Physics of Scale-Invariance: An Introduction." Fractals in the Earth Sciences. Philippe Baveye, Jean-Yves Parlange, and Bobby A. Steward (eds.). Florida: CRC Press, 1998, pp. 1-54.

Bray, J.W. and Hoek, E. Rock Slope Engineering. London: The Institute of Mining and Metallurgy, 1981.

Das, Braja M. Principals of Foundation Engineering. 5th ed. Pacific Grove: Brooks/Cole – Thompson, 2004.

Gabor, Korvin. Fractal Models in the Earth Sciences. Amsterdam: Elsevier Science Publishers, 1992.

Lambe, T. William and Robert V. Whitman. Soil Mechanics. New York: John Wiley and Sons, 1969.

Mandelbrot, Benoit B. Fractals: Form, Chance, ad Dimension. San Francisco: W.H. Freeman and Company, 1977.

Mandelbrot, Benoit B. The Fractal Geometry of Nature. San Francisco: W.H. Freeman and Company, 1982.

Russ, John C. Fractal Surfaces. New York: Plenum Press, 1994.

Vilimek, V., J. Kimes, J. Vlcko, and R. Carreno. "Catastrophic Debris Flows Near Machu Picchu Village (Aguas Calientes), Peru." Environmental Geology. 2006, pp. 1041-1052.

Vallejo, L.E., Sebastian Lobo-Guerrero, and Zamri Chik. "A Network of Fractal Force Chains and Their Effect in Granular Materials Under Compression." Fractals in Engineering. Jacques Levy-Vehel and Evelyne Lutton. Springer, 2005, pp. 67-80.

Vallejo, L.E. and James P. Hyslip. "Fractal Analysis of the Roughness and Size Distribution of Granular Materials." Engineering Geology. 1997, pp. 231-244.

Vallejo, L.E. "A Plane Stress Direct Shear Apparatus for Testing Clays" In: Geotechnical *Engineering Congress 1991*. F.G. McLean, D.A. Campbell, and D.W. Harris (eds.), Geotechnical Special Publication 27, Vol. II. American Society of Civil Engineers, pp. 851-862.

Von Daniken, Erich. Chariots of the Gods. New York: Bantam Books, 1971.

Wright, Kenneth R. and Alfredo Valencia Zegarra. Machu Picchu: A Civil Engineering Marvel. Reston, Virginia: ASCE Press, 2000.

Yoshida, Yojiro. "Force Chains and the Fragmentation of Granular Materials." Master's Thesis. Department of Civil and Environmental Engineering, University of Pittsburgh, 2004.

Zaniewski, John P. and Michael S. Mamlouk. Materials for Civil and Construction Engineers. Menlo Park: Addison Wesley Longman, Inc., 1999.